AGU ADVANCING EARTH AND SPACE SCIENCES

Tectonics®

Key Points:

- The relative amount of strain, pre-existing structures and rift accommodation zones influence the spatial variation of fault network topology at the rift-scale
- The connectivity of normal fault network is largely dependent on the fault network geometry, that is, the combination of the orientation and intensity of the faults
- Topological analysis of rift fault network provides a new, but complimentary way to characterize and distinguish large-scale structural domains in rift systems

Topological Characterization of a Fault Network Along the Northern North Sea Rift Margin

Edoseghe E. Osagiede[1,2] , Casey W. Nixon[1], Rob Gawthorpe[1] , Atle Rotevatn[1] , Haakon Fossen[1] , Christopher A.-L. Jackson[3] , and Fabian Tillmans[1,4]

[1]Geodynamics and Basin Studies Group, Department of Earth Science, University of Bergen, Bergen, Norway, [2]Department of Geology, University of Benin, Benin City, Nigeria, [3]Department of Earth Science & Engineering, Imperial College, London, UK, [4]Now at Equinor ASA, Sandsli, Norway

Abstract The factors that control the spatial variation of the topological characteristics of normal fault networks at the rift-scale are poorly understood. Here, we use 3D seismic reflection data from the northern North Sea to investigate the spatial variation of the geometry, topology, and strain heterogeneity of the Late Jurassic normal fault network along the rift margin. Our results show that fault orientation varies spatially along the rift margin. Normal faults within fault blocks that are adjacent to the North Viking Graben exhibits dominant N-S and NE-SW strikes that are sub-parallel to the graben axis and associated step-over, whereas in fault blocks farther from the graben, there is a dominant NW-SE strike. Furthermore, we identify two broad topological domains within the fault network: (a) dominated by isolated nodes, partially connected branches, and low fault connectivity, and (b) dominated by abutting nodes, fully connected branches, and moderate to high fault connectivity. These topological domains correlate with previous sub-division of the rift margin in the northern North Sea into platform and sub-platform structural domains, respectively. There is also a positive correlation between the spatial variability of the fault orientations and intensity, with the fault network connectivity, highlighting the relationship between normal fault geometry and topology. We conclude that the across and along-strike variation in strain, presence of pre-existing structures, and accommodation zone-related deformation are key factors influencing the spatial variation of fault network properties at the rift scale.

1. Introduction

Natural rift systems are characterized by complex networks of normal faults that exhibit a range of geometries and interaction patterns. The analysis of fault networks from natural rift systems, as well as those formed in physical and numerical models, demonstrate that several factors may control their complexity. Such factors may include the total amount of strain (e.g., Cowie & Scholz, 1992; Meyer et al., 2002), the number of extension phases driving deformation (e.g., Henza et al., 2010; Nixon, Sanderson, et al., 2014), local and regional variations of the causal stress field (e.g., Morley, 2017; Morley et al., 2007), the interaction and linkage of fault segments (e.g., Cartwright et al., 1995; Gawthorpe & Leeder, 2000), and/or the presence of inherited crustal heterogeneity (e.g., Daly et al., 1989; Dunbar & Sawyer, 1988; Henza et al., 2011; Osagiede et al., 2021; Reeve et al., 2015). For example, the multiphase rift history of the northern North Sea rift basin, in addition to the presence of pre-existing structures, likely influenced the present-day complexity of the rift fault network (e.g., Bartholomew et al., 1993; Duffy et al., 2015; Phillips et al., 2019; Reeve et al., 2015; Ziegler, 1975).

Characterizing the complexity of rift fault networks is important as it has implications for understanding rift-to-basin scale structural development, as well as seismicity in rift systems (e.g., Bell et al., 2009; Gabrielsen, 1986; Nicol et al., 2010; Sherman et al., 2004; Withjack et al., 2002). The complexity of fault networks may also control the geometry and integrity of structural traps and compartmentalize hydrocarbon, CO_2, and geothermal reservoirs (e.g., Aydin, 2000; Dimmen et al., 2017; Jolley et al., 2007, 2010; Leveille et al., 1997; Mulrooney et al., 2020; Ogata et al., 2014; Questiaux et al., 2010; Richards et al., 2015; Wu et al., 2021).

To describe and compare rift fault networks, we need to provide a detailed, qualitative and quantitative analysis of the geometry, kinematics, and the relationship between the individual faults in a fault network (e.g., Dershowitz & Einstein, 1988; Fossen, 2020; Manzocchi, 2002; Peacock et al., 2016; Sanderson & Nixon, 2015). Whereas most studies of natural fault networks have largely focused on the geometric (length, spacing, orientation, and frequency) and kinematic (strain history) evolution of the faults (e.g., Duffy et al., 2015; Ebinger, 1989; Gillespie et al., 1993; Meyer et al., 2002; Peacock et al., 2017), relatively few have considered the spatial arrangement and
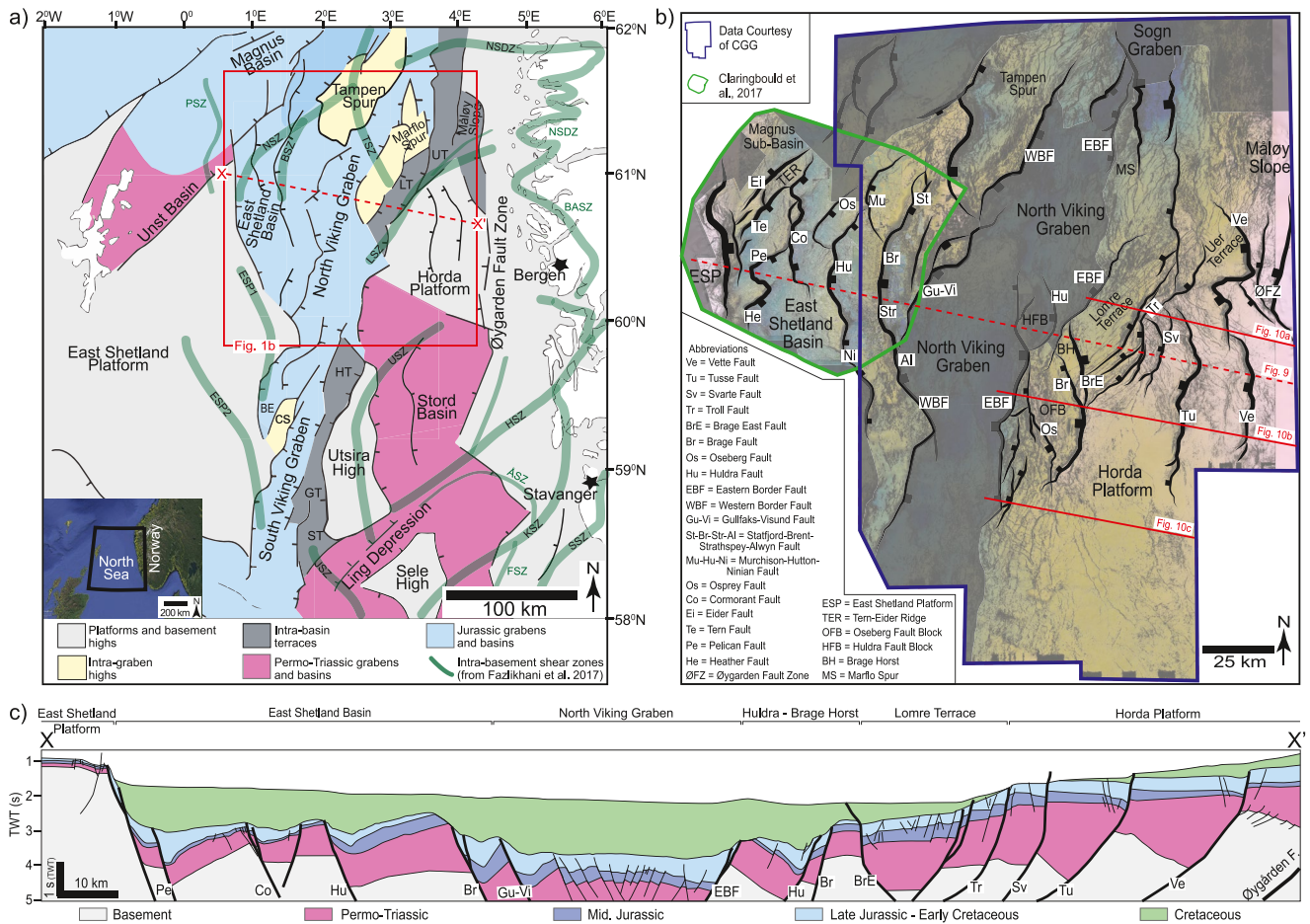
Figure 1. (a) Map of the key structural elements of the northern North Sea (after Riber et al., 2015; Osagiede et al., 2020), with the location of major pre-existing Devonian shear zones (thick green lines) indicated (after Fazlikhani et al., 2017). (b) Major faults within our study area (red box in a) interpreted at near-Top Brent structural level (time-structure map in background). The transparent gray areas represent the areas excluded from the rift fault network analysis (see text for details). (c) Regional cross-section (stipple lines X–X' in a and b) across the East Shetland Platform, East Shetland Basin, North Viking Graben, Brage Horst, Lomre Terrace, and Horda Platform. (See the web version for references to colors).

connectivity between these individual structures, that is, the "fault network topology" (Duffy et al., 2017; Morley & Nixon, 2016; Sanderson & Nixon, 2018). Furthermore, these studies have only investigated rift fault network topologies at limited scales of a few 10 to 100 s of km², with little or no focus on the spatial variation of the network properties. Consequently, the spatial distribution of fault network topology at rift-scale (i.e., 1,000 s of km²) and the controls of spatial variations are poorly understood.

In this paper, we characterize the complexity of the regional fault network along the rift margin of the northern North Sea rift system using regionally extensive 3D reflection seismic survey (Figure 1). Specifically, we (a) constrain the planform spatial distribution of the geometry, intensity, and topology of the fault network at the rift-scale, (b) examine the inter-relationship between the fault network geometry, topology, and strain heterogeneity, and (c) assess the factors that control the topological character of the fault network. Our results have implication for understanding the spatial development of connectivity and compartmentalization in rift fault networks, and for the characterization of large-scale structural domains in rifts.

2. Regional Geological Setting

The northern North Sea rift basin developed in response to multiple phases of crustal extension that occurred between the Late Paleozoic and Middle Mesozoic (e.g., Badley et al., 1988; Bartholomew et al., 1993; Coward et al., 2003; Færseth, 1996; Ziegler, 1992). The northern North Sea rift basin extends from the East Shetland Basin in the west to the Horda Platform in the east, with the East Shetland Platform and Øygarden Fault Zone defining its western and eastern limits, respectively (Figure 1a; Odinsen et al., 2000; Lervik, 2006).

The northern North Sea has undergone at least two major rift phases (e.g., Badley et al., 1988; Bartholomew et al., 1993; Bell et al., 2014; Færseth, 1996; Nøttvedt et al., 1995; Odinsen et al., 2000; Ziegler, 1990). The first phase occurred during the Late Permian to Early Triassic, concurrently with the breakup of the Pangea supercontinent (Coward et al., 2003; Færseth, 1996; Ter Voorde et al., 2000; Ziegler, 1992). This phase led to the development of widespread graben and half-graben basins across the East Shetland Basin and the Horda Platform (Figure 1a; Færseth, 1996). The predominant N-S orientation of these basins and their bounding faults (Bell et al., 2014; Færseth, 1996; Roberts et al., 1995), and the presence of N-striking Permian dykes onshore western Norway (Fossen & Dunlap, 1999; Torsvik et al., 1997), reflect an E-W regional extension direction during the Permo-Triassic rift phase (Fossen, 1998; Valle et al., 2002). Overall, the stratigraphy consists mainly of continental red beds of interbedded sandstones and mudstones/claystones of the Hegre Group, deposited in response to the Early Triassic uplift of the Fennoscandian Shield and the regression of the Arctic Sea (Lervik, 2006; Ziegler, 1992).

Several authors suggest that a tectonically dormant (inter-rift) period, when lithospheric thermal cooling rather than slip on rift-related faults drove subsidence, followed the Permian-Triassic rift phase, lasting until the Middle Jurassic (e.g., Badley et al., 1988; Bartholomew et al., 1993; Coward et al., 2003; Ziegler, 1990). However, more recent studies suggest that the rift-related faults may not have been completely inactive during this period (Claringbould et al., 2017; Deng et al., 2017). An Early-Middle Jurassic thermal doming event (Davies et al., 1999; Underhill & Partington, 1993; Ziegler, 1992) and associated uplift in the central North Sea, is also thought to have driven increased sediment supply and the development of a large deltaic system, resulting in the deposition of the Middle Jurassic Brent Group over the northern North Sea rift basin (Helland-Hansen et al., 1992; Mitchener et al., 1992; Underhill & Partington, 1993).

The second major rift phase in the northern North Sea occurred during the Middle Jurassic to Early Cretaceous (Badley et al., 1988; Bell et al., 2014; Færseth & Ravnås, 1998; Ziegler, 1975). The collapse of the Middle Jurassic thermal dome and far-field stresses associated with the Arctic–North Atlantic rift system likely drove Middle Jurassic–Early Cretaceous rifting (Underhill & Partington, 1993; Ziegler, 1992). Fault displacement measurements and lateral changes in the thickness of Middle-Late Jurassic strata reveal that during the second rift phase, most of the deformation in the northern North Sea rift localized along the Viking Graben (Figure 1c; Bell et al., 2014). Middle Jurassic–Early Cretaceous rift-related faults have a predominant N-S strike although c. NE-SW striking faults are also common (Færseth et al., 1997); this has caused a long-lived debate about the regional extension direction during this rift second phase. Recent kinematic analyses of Middle Jurassic faults, however, show that both N-S and NE-SW striking faults initiated coevally (Osagiede et al., 2020; Reeve et al., 2015), suggesting that the regional extension direction may not have changed. That is, whereas N-S striking faults nucleated in response to regional E-W extension direction, the NE-SW striking faults nucleate in response to localized stress perturbation driven by pre-existing heterogeneities (Bartholomew et al., 1993; Osagiede et al., 2020). The Middle Jurassic–Early Cretaceous stratigraphy consists of the Viking Group, which comprises deep-marine mudstone units of the Heather and Draupne/Kimmeridge clay Formations, interbedded with shallow marine and deltaic sand-rich units of the Krossfjord, Fensfjord, and Sognefjord formations (Dreyer et al., 2005; Holgate et al., 2013; Patruno et al., 2015; Ravnås & Bondevik, 1997; Tillmans et al., 2021).

Although the present configuration of the northern North Sea rift basin is a product of these two major rift episodes, the inherited intra-basement structural template upon which they developed plays an important role. The basement consists of Proterozoic to Devonian rocks (e.g., Ksienzyk et al., 2013; Slagstad et al., 2011) deformed during the Caledonian orogeny, and Devonian post-orogenic extensional collapse (Dewey, 1988; Fossen, 1992; Gee et al., 2008; Glennie, 1986; McKerrow et al., 2000; Wiest et al., 2021; Ziegler, 1975). The post-orogenic collapse and extension led to the reactivation of low-angle thrust and the development of large, pre-rift, extensional shear zones (e.g., Fossen, 1992), that exerted a variable influence on the geometry and evolution of the major rift phases in the northern North Sea (e.g., Bartholomew et al., 1993; Fazlikhani et al., 2017; Fossen et al., 2017; Johnson & Dingwall, 1981; Osagiede et al., 2020; Phillips et al., 2016, 2019; Platt, 1995; Reeve et al., 2013; Wiest et al., 2020).

In this study, we focus on the Middle Jurassic near-Top Brent structural level, which post-dates the climax of rift phase 1, and marks the possible onset of rift phase 2 (e.g., Bell et al., 2014). Consequently, with respect to both rift phases, the near-Top Brent is affected by both the reactivated older Permo-Triassic, and the younger newly formed Middle Jurassic–Early Cretaceous rift faults (e.g., Duffy et al., 2017), thus allowing for the detailed characterization of the fault network along the rift margin.
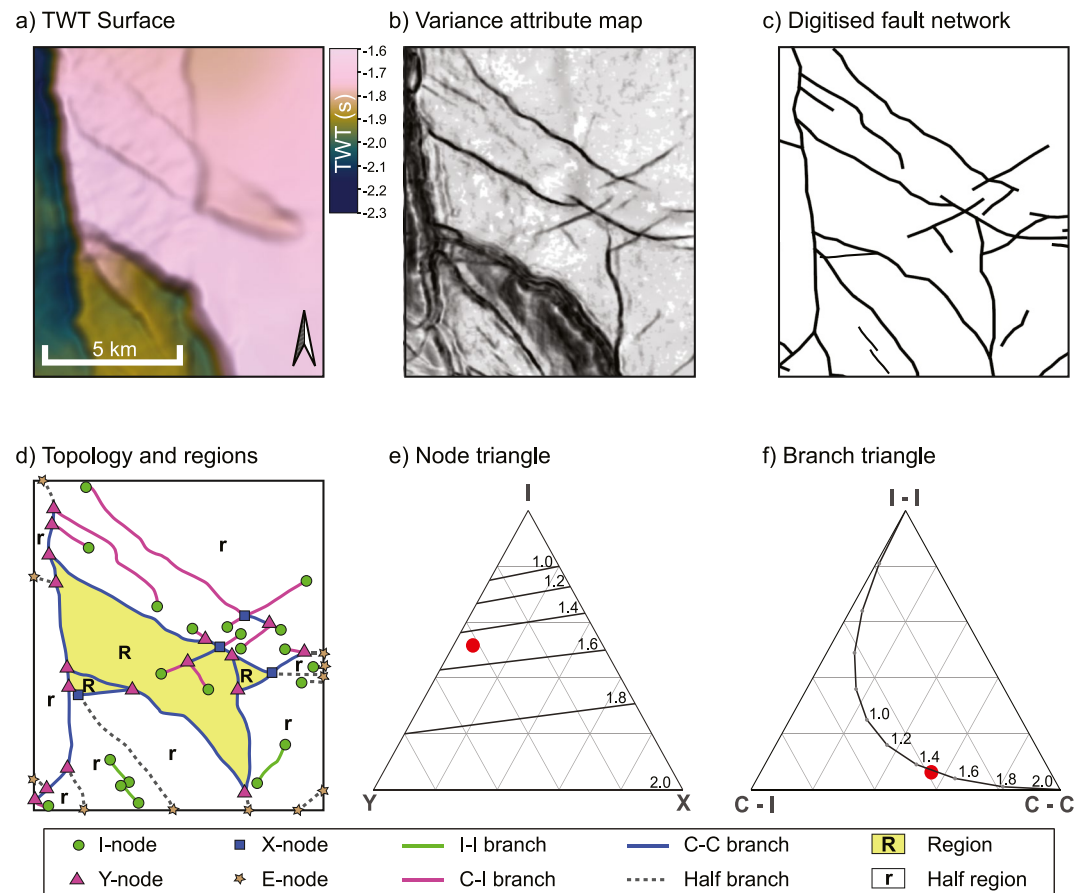
Figure 2. (a) Representative two-way time (TWT) map of the near-Top Brent surface. (b) Corresponding variance attribute map extracted from the TWT map highlighting the rift faults. (c) Digitized polyline traces of the rift fault network. (d) Topology of the network showing the different types of nodes and branches, and the regions. Panels (e) and (f) are the node and branch ternary diagrams, respectively, showing where the rift fault network in (d) plots topologically based on the proportions of the nodes and branches (small red circles).

3. Data Set and Methods

3.1. Seismic Reflection Data and Interpretation

We use two overlapping, high-quality, 3D seismic reflection volumes, covering an extensive (c. 39,000 km^2) region comprising the Horda Platform and Måløy Slope (to the east), the North Viking–Sogn Graben, and the Tampen Spur and East Shetland Basin areas (to the west) (Figure 1b). The largest 3D seismic volume is from broadband data provided by CGG (CGG Broadseis); this has an areal coverage of c. 35,000 km^2 (Figure 1b). The broadband data is a single data set that was collected and processed as a continuous, homogeneous survey. The data is post-stack depth migrated and has been time-stretched so that the *z*-axis corresponds to depth in two-way time (TWT). The data has 18.75×12.5 m inline and crossline spacing and images to a depth of up to 9 s TWT. The other 3D seismic volume is a merged survey covering an area of c. 5,000 km^2 of the East Shetland Basin on the western margin (Claringbould et al., 2017). The data is post-stack time migrated with an inline and crossline spacing of 12.5 m, and depth imaging to 5 s TWT.

We extracted variance seismic attribute on a near-Top Brent surface (in two-way-time), mapped over the two seismic volumes (e.g., Figures 2a and 2b). Variance is a useful seismic attribute for detecting relatively small-scale seismic faults, since it compares the continuity of seismic waveforms between neighboring traces (e.g., Chopra & Marfurt, 2005). Using the near-Top Brent variance attribute surface as a base map, faults along the eastern and western rift margins were digitized in ArcGIS using their footwall cut-offs as a 2D network of polyline traces (Figure 2c). The interpretation also involved checking the faults on cross-sectional seismic sections.

Despite the exceptional high quality of the 3D seismic reflection data, there is still a need to address the potential limitations imposed by the data and acknowledge any uncertainties when mapping the fault network. The reso-

lution and/or quality of seismic reflection data have been recognized as a key limitation when interpreting fault networks (e.g., Morley & Nixon, 2016; Nixon et al., 2012; Pickering et al., 1997; Watterson et al., 1996). This is because (a) faults with small displacement may be below seismic detection and are thus not accounted for in the fault network, and (b) the length of individual faults may be underestimated because the true lateral fault tip is sub-seismic and different from the seismically mapped fault tip. Both can lead to underestimates of the absolute abundances and connectivity of faults (Espejel et al., 2020; Nixon et al., 2012; Pickering et al., 1997). Since our focus is on the relative spatial distribution of the fault network properties, our results are less affected by the absence of unresolvable smaller faults. Furthermore, the high resolution of the data also helps minimize this limitation. With regards to mapping lateral fault tips, the vertical and lateral seismic resolution of our 3D seismic reflection data set, at the depth corresponding to the Jurassic near-Top Brent structural level, is estimated as c. 15 and 30 m, respectively (Tillmans et al., 2021). Thus to address this limitation, we extended the seismically mapped fault tips by up to 30 m or until a fault intersects another, following the recommendation of Pickering et al. (1997).

Additional uncertainty arises from local reductions in the seismic data quality and imaging, either in areas of low/no data coverage due to large hydrocarbon field installations (particularly around the Gullfaks Field on the western rift margin of the study area), areas of intense erosion at the near-Top Brent interval on the eastern Måløy Slope, or where the near-Top Brent horizon is deeply buried such as the North Viking and Sogn grabens (Figure 1b, see also Figure S1 in Supporting Information S1). To address the latter, the eastern Måløy Slope and the deep graben areas were excluded from the analysis. Despite the limitation imposed by the data quality and resolution, the results we present in this study are of unprecedented detail, providing significant insights into the spatial distribution of the geometric and topological properties of a complex fault network at the rift-scale.

3.2. Network Topology and Compartmentalization

We use "*node* and *branch*" topology (Manzocchi, 2002; Sanderson & Nixon, 2015) and the identification of *regions* (Sanderson et al., 2019) to analyze the 2D fault network at near-Top Brent structural level in the northern North Sea rift system. These approaches have been described in detail by Sanderson and Nixon (2015) and Sanderson et al. (2019), thus we provide only a summary here.

In map-view, a *node* is a point that represents the tip or intersections of faults, and can either be an isolated-tip (I-node), splaying/abutting (Y-node), or cross-cutting (X-node), whereas a *branch* is a line that connects two neighboring nodes (Figure 2d; e.g., Manzocchi, 2002; Sanderson & Nixon, 2015). Branches can be classified into: (a) isolated (I-I), (b) partially connected (I-C), and (c) fully connected (C-C) branch types, where C (connected node) represents either a Y- or X- node (Sanderson & Nixon, 2015). The amount and relative proportion of the nodes and branches allow for the characterization of a fault network, and the determination of other important topological parameters such as the average number of connections per branch (C_B) and connecting node frequency (N_c/m^2) that relates to the degree of connectivity of a network (e.g., Manzocchi, 2002; Nyberg et al., 2018; Sanderson & Nixon, 2015). Quantitatively, C_B and connecting node frequency are given as;

$$C_B = (3N_Y + 4N_X)/N_B \qquad (1)$$

$$\text{Connecting node frequency} = N_C/A \qquad (2)$$

Where N_Y is the number of Y-nodes, N_X is the number of X-nodes, N_B is the number of branches, N_C is the number of connecting nodes, and A is the sample area.

A *region* represents a block of rock completely bounded by connecting branches within a connected component (Figure 2d; e.g., Huseby et al., 1997; Sanderson et al., 2019; Nixon et al., 2020). Using a generalized Euler's theorem, the number of regions (N_R) is related to the number of components (N_K), number of nodes (N_N), and number of branches (N_B) by the equation (see Sanderson et al., 2019; Nixon et al., 2020 for detailed derivation):

$$N_N - N_B + N_R - N_K = 0 \qquad (3)$$

Therefore,
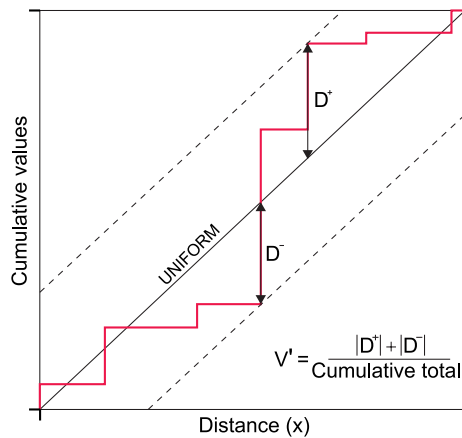
$$N_R = N_B - N_N + N_K \qquad (4)$$

Figure 3. The modified Kuiper's test showing cumulative plot (red line) over distance along a sample line. D$^+$ and D$^-$ represents the maximum deviation above and below the uniform distribution (black solid line).

More importantly, N_R in relation to the sample area allows for the derivation of the dimensionless block intensity (R_{22}; *sensu* Nixon et al., 2020). R_{22} provides a measure of the relative amount of brokenness/deformation of the rock mass, and range in value from 0 (highly broken up/deformed) to 1 (intact) (Nixon et al., 2020). Furthermore, identified regions provide a basis for quantifying the amount of fault-enclosed compartments of rift fault networks.

The digitized fault network was analyzed using the open source NetworkGT GIS toolbox by Nyberg et al. (2018), which automatically extracts relevant geometrical (e.g., length and orientation distribution, fault intensity) and topological (e.g., nodes and branches, connectivity) attributes. To adequately assess and compare the spatial variability of the geometry and topology within the northern North Sea fault network, we used a combination of both area sub-sampling and contour grid maps of key network properties such as fault intensity and connectivity (*sensu* Nyberg et al., 2018). The area sub-sampling was achieved by subdividing the rift margin fault network into sub-areas defined by major fault-bounded blocks, leading to a more systematic spatial correlation of the network geometry. On the other hand, the contour grid maps define a regular grid of fixed cell sizes and a search radius, depending on the spatial distribution of the faults, that allows for a continuous and quantitative analysis of the network properties (e.g., Nyberg et al., 2018). For this study, we used a contour grid size of 2×2 km and a search radius of 8 km (see Figure S2 in Supporting Information S1).

3.3. Spatial Heterogeneity Analysis of Faulting and Strain

We used the modified Kuiper's test to assess the spatial heterogeneity of faulting and strain within the fault network (Putz-Perrier & Sanderson, 2008). The modified Kuiper's test compares the cumulative plot of fault frequency and throw to a uniform cumulative distribution function represented by a straight line (Figure 3; e.g., Putz-Perrier & Sanderson, 2008). The method calculates a normalized non-parametric heterogeneity parameter $V' = |D^+| + |D^-|/T$, where D^+ and D^- are the maximum deviation above and below the uniform distribution line, respectively, and T is the cumulative number of either the faults or amount of throw, for frequency V'_f analysis and strain V'_s analysis, respectively (Putz-Perrier & Sanderson, 2008). The values of V'_f and V'_s range from 0 to 1, with the degree of heterogeneity of faulting and strain increasing as V' increases toward 1.

The frequency and vertical displacement (throw) of every seismically resolvable fault that offset the near-Top Brent surface were measured along WNW-ESE oriented transects that were approximately perpendicular to the graben axis (Figure 1b; see Figures S3–S6 in Supporting Information S1 for the seismic sections). The longest Transect X runs from the East Shetland Basin to the Horda Platform, allowing us to compare the heterogeneity parameter of both the western and eastern rift margins of the North Viking Graben. The other three transects (A, B, and C) have a spacing of c. 40 km, and are located in the northern, central, and southern parts of the Horda Platform, thus sampling variations in the spatial distribution of faulting and strain along-strike of the rift margin. The effect of hangingwall drag and footwall erosion on the throw measurement were eliminated by projecting the attitude of the surface outside of the drag or eroded zone on to the fault (Mansfield & Cartwright, 1996). Throw values were also converted to depth (in meters) using an interval velocity of 3,200 m/s for the Brent Group, following Jackson et al. (2010). A Terzaghi correction factor was applied to the measured throw values, to account for the angle between the strike of the faults and the sample lines (Terzaghi, 1965).

4. Geometry, Topology, and Strain Heterogeneity of the Northern North Sea Rift Margin Fault Network

We present the results of the geometrical, topological, and strain heterogeneity analysis of fault network in the eastern and western rift margins of the northern North Sea. The eastern rift margin covers the area east of the Viking and Sogn graben, notably the Horda Platform and the Måløy Slope areas (Figure 1b). We divided the eastern rift margin fault network into 10 major fault blocks, which are used as sub-sampling polygons. These fault blocks are either completely bounded by major faults (with c. ≥500 m of vertical displacement) or also by the edge of the study area (Figure 4). The fault blocks are named; Horda Platform 1–4, Oseberg, Brage Horst, Lomre
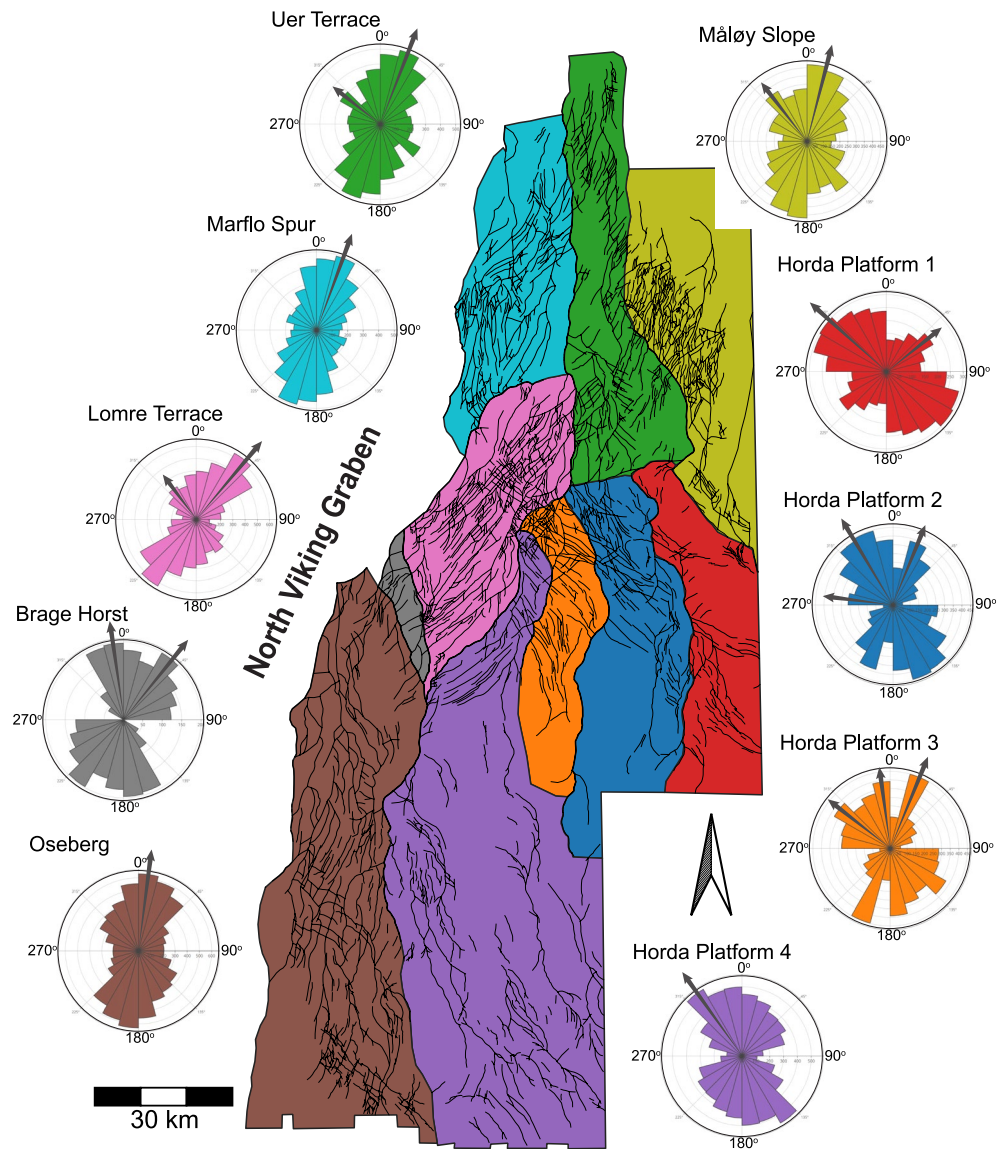
Figure 4. Fault network of the eastern rift margin. The different colored areas are the fault block polygons used to assess the variation of the fault orientation represented by the rose diagrams.

Terrace, Marflo Spur, Uer Terrace, and Måløy Slope (Figure 4; see Table S1 in Supporting Information S1 for reference to the major faults bounding the fault blocks).

The western rift margin covers the East Shetland Basin, the north-eastern edge of the East Shetland Platform, the Magnus Sub-Basin, and the Tampen Spur area of the study (Figure 1b). Like the eastern margin, we divided the margin into 13 fault blocks bounded by major faults. The fault blocks are named: East Shetland Platform, Magnus Sub-Basin, Tern-Eider Ridge, East Shetland Basin 1–7, Gullfaks, and Tampen Spur 1 and 2 (Figure 5; see Table S1 in Supporting Information S1 for reference to the major faults bounding the fault blocks).

4.1. Major and Minor Fault Orientations on the Northern North Sea Rift Margins

On the eastern rift margin, fault orientation is variable between the fault blocks. In general, the fault blocks adjacent to the North Viking Graben (i.e., Oseberg, Brage Horst, Lomre Terrace, Marflo Spur) have main orientations
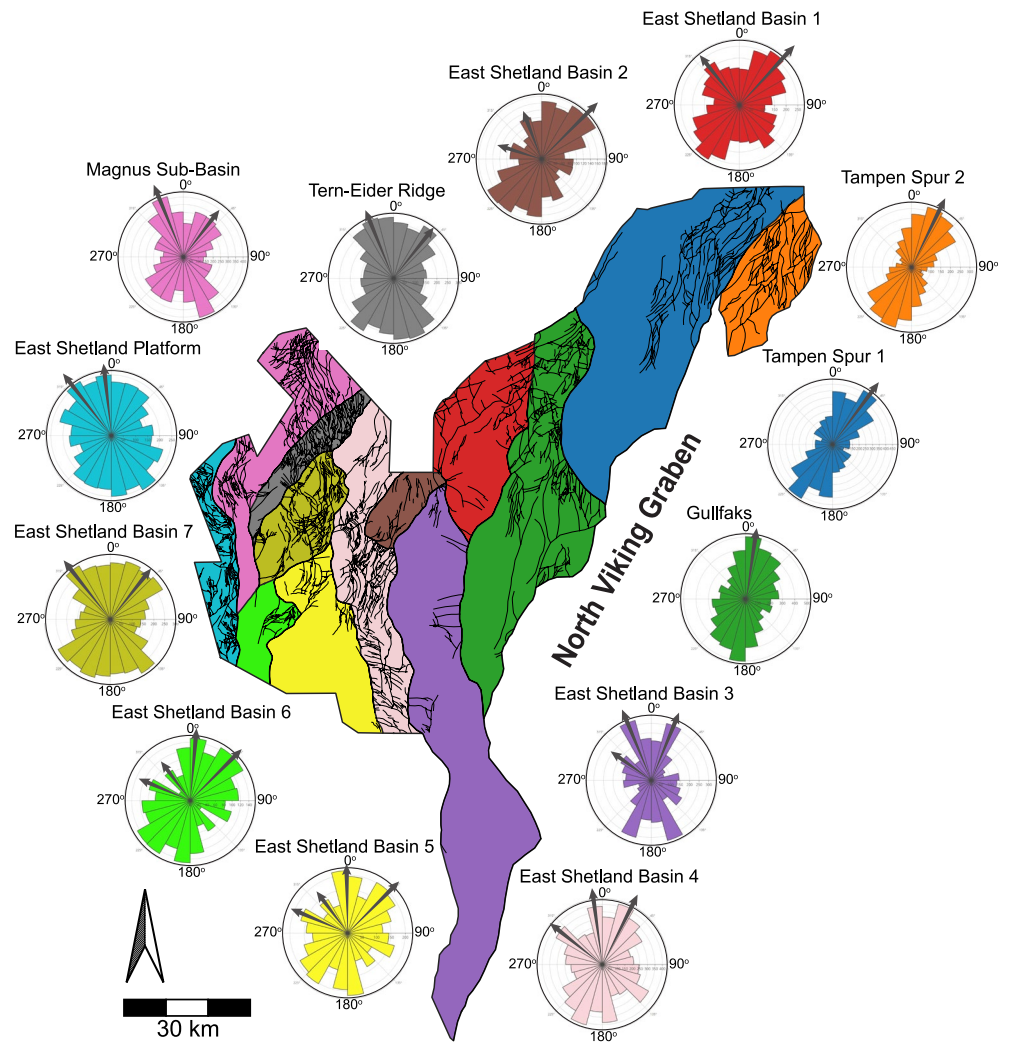
Figure 5. Fault network of the western rift margin. The different colored areas are the fault block polygons used to assess the variation of the fault orientation represented by the rose diagrams.

that are sub-parallel to the rift axis, which varies from a N-S orientation in the Oseberg Block, to a dominant NE-SW orientation on the Lomre Terrace, to a NNE-SSW orientation on the Marflo Spur (Figure 4). The Brage Horst exhibits two equally weighted orientations (N-S and NE-SW), representing a transition between the dominant orientations of the Oseberg Block and the Lomre Terrace (Figure 4). Further away from the North Viking Graben, the fault orientations become more variable within the different fault blocks. In addition, there is often a minor NW-SE orientation, particularly within the Uer Terrace, Maløy Slope, and Horda Platform 3 fault blocks, but it becomes the dominant orientation within Horda Platform 1, 2, and 4 fault blocks (Figure 4). The most complex fault orientations are found within the Horda Platform 2 and 3 fault blocks, which are adjacent to the Lomre Terrace where the rift margin steps to the right (Figure 4).

Fault orientations also vary spatially between the fault blocks on the western rift margin (Figure 5). Like the eastern rift margin, the fault blocks adjacent to the North Viking Graben (i.e., Gullfaks, Tampen Spur 1 and 2) generally have fault orientations that are sub-parallel to the rift axis, varying from a N-S orientation on the Gullfaks block, to a dominant NE-SW- and NNE-SSW- orientations on the Tampen Spur fault blocks, respectively (Figure 5). Further from the North Viking Graben, into the East Shetland Basin blocks, the fault orientations are more variable and complex, with minor NW-SE to WNW-ESE orientations occurring in addition to the dominant rift parallel orientations, especially within most of the East Shetland Basin fault blocks (Figure 5). However,
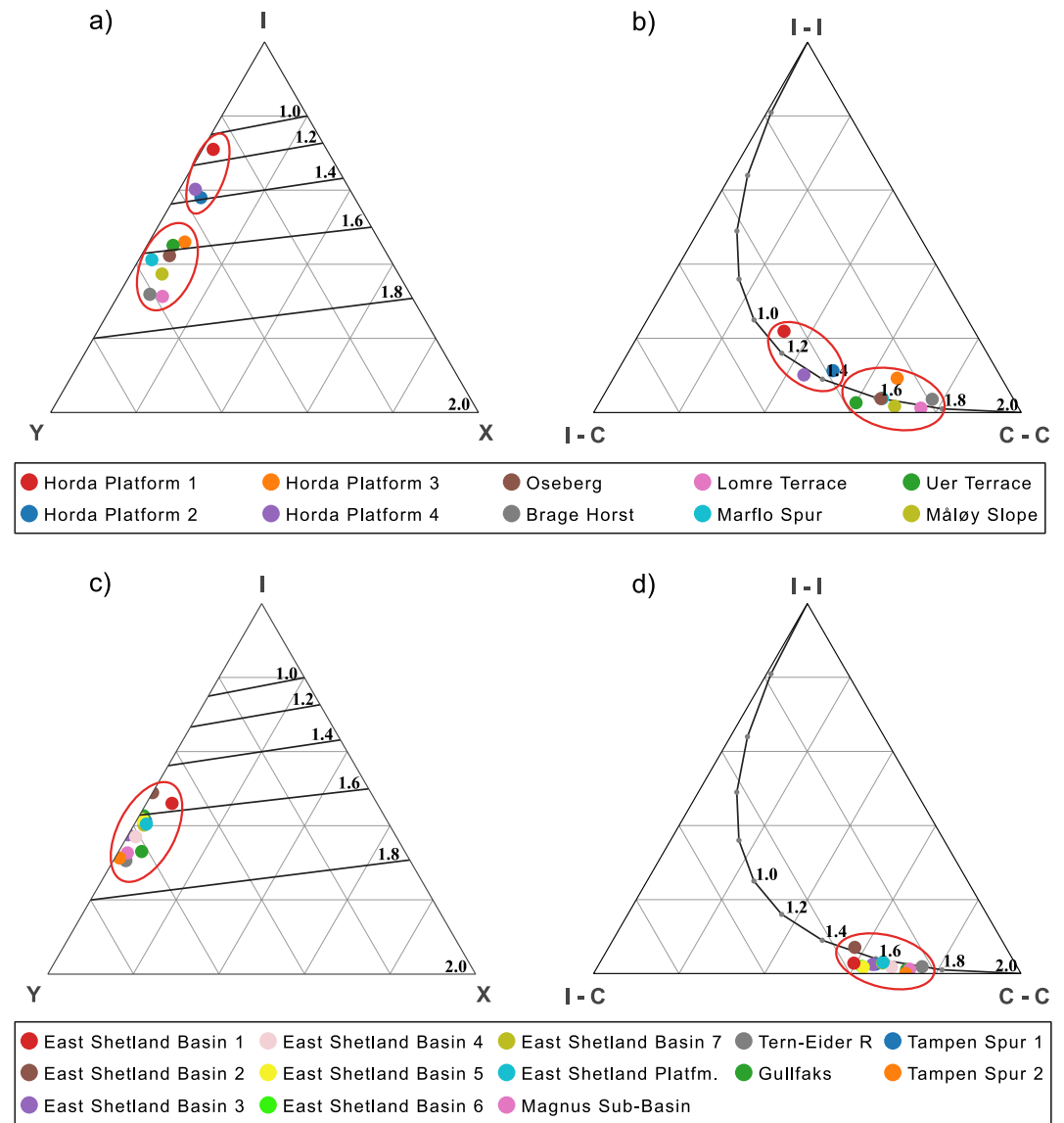
Figure 6. Node and branch ternary plots of the rift margin fault blocks. (a) Node ternary plot of the eastern margin based on the proportions of I-, X-, and Y- nodes. (b) Branch ternary plot of the eastern margin based on the proportions of I-I, I-C, and C-C branches. (c) Node ternary plot of the western margin based on the proportions of I-, X-, and Y- nodes. (d) Branch ternary plot of the western margin based on the proportions of I-I, I-C, and C-C branches. The topological domains/clusters are indicated by the red circle.

the minor NW-SE orientation becomes more dominant within the most distal fault blocks, that is, East Shetland Basin 7, Tern-Eider Ridge, Magnus Sub-Basin, and the East Shetland Platform fault blocks (Figure 5).

4.2. Fault Network Topology

4.2.1. Node and Branch Topology of the Rift Margin Fault Blocks

We summarize the topologies of the different fault blocks as ternary plots (Figure 6), based on the relative proportions of the different types of nodes and branches (Table 1). In general, the fault network shows low proportions of X-nodes, plotting close to the I-Y axis of the node ternary plot (Figures 6a and 6c), a common observation for rift fault networks (e.g., Morley & Nixon, 2016; Nixon et al., 2012). On the eastern rift margin, Horda Platform 1 fault block has the highest proportion of isolated I-nodes (71%), whereas the Lomre Terrace has the highest proportion of connecting nodes (i.e., X- and Y-nodes; 11% and 58%, respectively; Table 1). The nodal topology

Table 1
Topology Data of Each of the Fault Blocks in the Eastern and Western Rift Margins, Indicating the Proportions of the Different Node and Branch Types and the Connections per Branch (C_B)

Fault block	Nodes (%)			Branches (%)			
	I	X	Y	C-C	C-I	I-I	C_B
Eastern margin							
Horda Platform 1	71	3	26	34	44	22	1.12
Horda Platform 2	58	6	36	50	39	11	1.39
Horda Platform 3	46	8	46	66	24	10	1.57
Horda Platform 4	60	4	36	44	46	10	1.34
Oseberg	42	7	51	65	31	4	1.62
Brage Horst	32	7	61	77	19	4	1.74
Lomre Terrace	31	11	58	76	23	1	1.75
Marflo Spur	41	3	56	66	30	4	1.63
Uer Terrace	45	6	49	60	37	3	1.58
Måløy Slope	37	8	55	69	29	2	1.68
Western margin							
East Shetland Platform	40	3	57	66	31	3	1.63
Magnus Sub-Basin	33	2	65	73	26	1	1.72
Tern-Eider Ridge	31	3	66	76	22	2	1.75
East Shetland Basin 1	46	6	48	59	38	3	1.57
East Shetland Basin 2	49	0	51	58	35	7	1.52
East Shetland Basin 3	38	0	62	64	34	2	1.67
East Shetland Basin 4	37	2	61	69	29	2	1.67
East Shetland Basin 5	42	1	57	62	36	2	1.62
East Shetland Basin 6	43	1	56	62	36	2	1.60
East Shetland Basin 7	40	2	57	66	31	3	1.64
Gullfaks	33	5	62	73	26	1	1.72
Tampen Spur 1	41	2	57	65	33	2	1.62
Tampen Spur 2	31	1	68	73	27	0	1.74

Note. An extended table with the raw numbers of nodes and branches is presented in Table S2 in Supporting Information S1.

of fault blocks forming the platform area (Horda Platform 1, 2, and 3) is dominated by I-nodes and forms a topological domain/cluster (Figure 6a), whereas the fault blocks forming the terraces (e.g., Lomre Terrace) are more Y-node dominated and forms a second topological domain/cluster (Figure 6a). The branch topology indicates that the fault blocks forming the terraces are dominated by C-C branches, whereas the fault blocks from the platform area have relatively more I-C and I-I branches (Figure 6b and Table 1). This indicates that the platform areas contain more isolated faults and fault splays, whereas the terraces exhibit more interconnected networks. Indeed, the terraces exhibit a high degree of network connectivity with values for the connections per branch (C_B) ranging from 1.58 for the Uer Terrace to 1.75 for the Lomre Terrace. In contrast, the platform area exhibits a relatively low degree of network connectivity with C_B ranging from 1.12 to 1.57 (Table 1).

On the western rift margin, all the fault blocks are Y-node dominated, forming a similar cluster as the terraces on the eastern margin (Figure 6c). Tampen Spur 2 fault block has the highest proportion of Y-nodes (68%), whereas the East Shetland Basin 1 has the highest proportion of X-nodes (6%; Table 1). The fault blocks contain interconnected fault networks dominated by C-C branches, with the overall values of $C_B > 1.5$ (Figure 6d and Table 1). The Tern-Eider Ridge fault block, which is an intra-basin horst block, is the most connected ($C_B = 1.75$), with the highest proportion of C-C branches (Table 1).
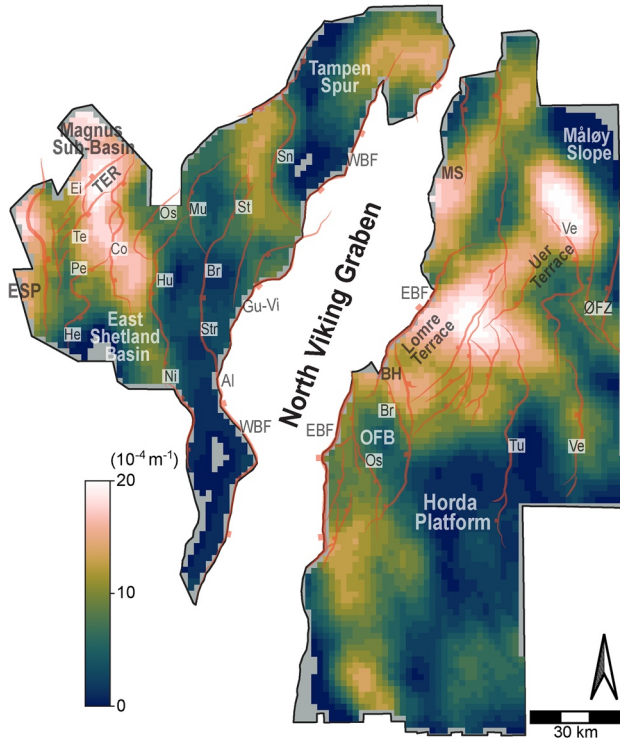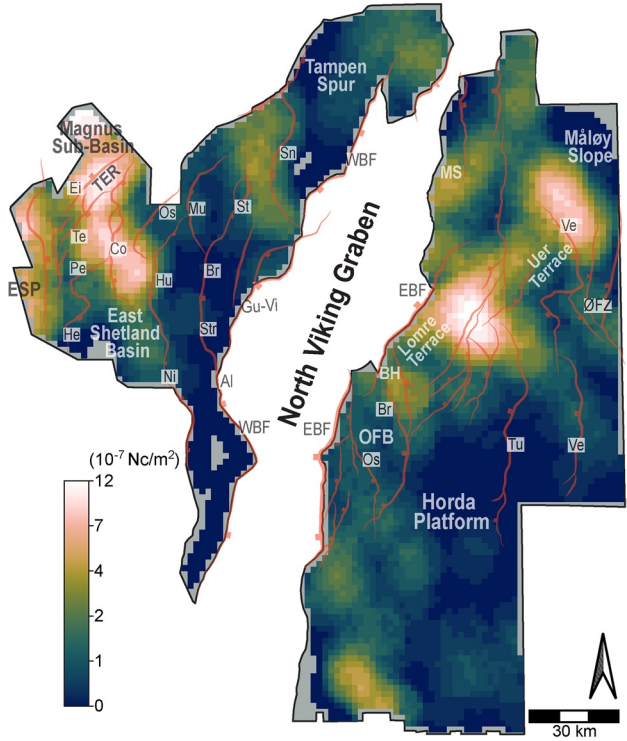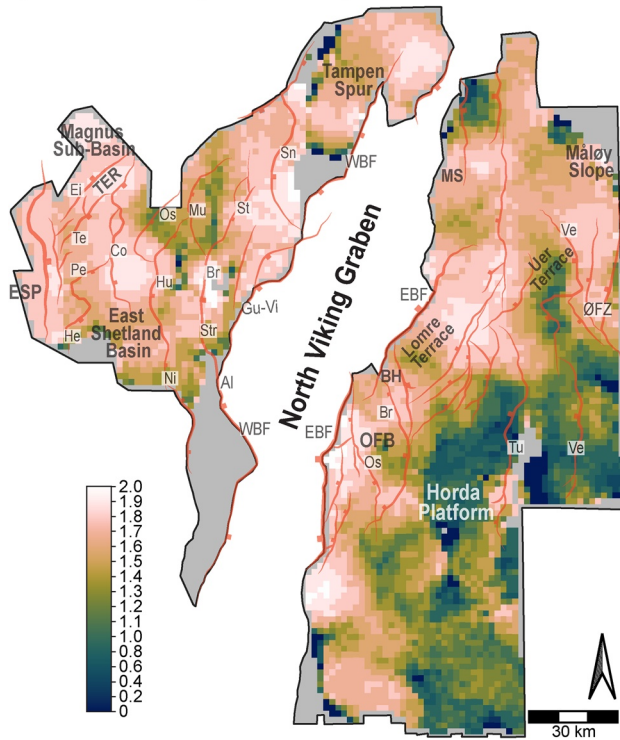
Figure 7. Contour maps of the spatial distribution of rift fault network properties in the eastern and western margins of the North Viking Graben. (a) 2D fault intensity, showing the spatial variation in the relative abundance of the rift faults. (b) Connecting node frequency and (c) dimensionless connections per branch (C_B), showing the spatial variation in the relative connectivity of the network. Note the overall positive correlation in the pattern of spatial distribution of the different network properties. The major faults and structural elements are indicated for easy reference to locations. See Figure 1b for definition of abbreviations.

4.2.2. Spatial Mapping of Fault Network Properties

The contour grid plots of the fault intensity, connecting node frequency and connection per branch (C_B) of the rift fault network, are presented in Figure 7. On the eastern rift margin, there is generally lower fault intensity in the south, especially around the Horda Platform, compared to the north on the Lomre Terrace and Måløy Slope. In the south, fault intensity shows a clear decrease with increasing distance from the North Viking Graben (Figure 7a). Whereas in the north, fault intensity is more variable with two areas of high fault intensity located on the Lomre Terrace and Måløy Slope (Figure 7a). These two areas of high fault intensity are linked by a NE-SW-striking zone of high fault intensity. Farther north, there is another zone of high fault intensity with a similar NE-SW strike across the Marflo Spur (Figure 7a). Spatial patterns in the connecting node frequency generally correlate positively with the fault intensity, such that the areas of highest connecting node frequency coincide with the two areas of highest fault intensities observed on the Lomre Terrace and Måløy Slope, respectively (compare Figures 7b and 7a). Like the pattern of fault intensity, there is a NE-SW-striking zone of high-intermediate connecting node frequencies that link the two areas (Figure 7b). The spatial distribution of C_B shows broadly higher values close to the North Viking Graben and decreases away from the graben (Figure 7c). Values for C_B are lowest to the southeast on the Horda Platform (generally <1.5) and there is a local high in C_B around the Lomre Terrace (Figure 7c). This is similar to the node and branch topology of the fault blocks with differences between the platform area and the terraces (Figure 6b).

On the western rift margin there is also a positive correlation in the spatial variability of fault intensity and connecting node frequency (compare Figures 7a and 7b). Fault intensity and connecting node frequency tends to increase with increasing distance from the North Viking Graben, except in the Tampen Spur area to the north (Figures 7a and 7b). In contrast to the eastern rift margin where the high fault intensity and connecting node frequency zones have a NE-SW strike, the high fault intensity and connecting node frequency zones on the western rift margin have an approximately N-S strike (Figures 7a and 7b). The most prominent N-S striking zone starts from the Magnus Sub-basin, crosses the Tern-Eider Ridge, and extends into the East Shetland Basin (Figures 7a and 7b). Unlike fault intensity and connecting node frequency, values of C_B show little spatial variability with values broadly ≥1.5 indicating overall moderate to high degree of connectivity (Figure 7c). These values of C_B compares well with the values observed in the eastern rift margin, excluding the Horda Platform (Figure 7c).

4.2.3. Patterns in Fault Compartmentalization

Contour grid plots of the dimensionless block intensity (R_{22}) indicate the amount of fault-enclosed compartments and thus quantify how deformed or intact the margins are at the near Top Brent level. On both the eastern and western rift margins, the variation of R_{22} follows the pattern of variation in fault intensity and connecting node frequency, albeit with an inverse correlation, that is, the areas of low R_{22} correlate with areas of high fault intensity and connecting node frequency (cf. Figure 8a with Figures 7a and 7b). On the eastern rift margin there are two areas of relatively low R_{22} (≤0.01) around the Lomre Terrace and on the Måløy Slope (Figure 8a). These low R_{22} areas indicate zones of relatively high deformation. Values of R_{22} generally increase with increasing distance away from the eastern margin of the North Viking Graben, which indicates less deformation away from the graben axis (Figure 8a). Indeed, the map of the spatial distribution of fault-enclosed compartments (Figure 8b), show that the Horda Platform is characterized by a negligible number of compartments that are spatially extensive. In contrast, along-strike from the Oseberg to Marflo Spur consist of numerous moderate- to small-sized compartments. Notably, is the cluster of small-sized compartments around the Lomre Terrace (Figure 8b), which corresponds with the area of lowest R_{22} values (Figure 8a), indicating a relatively high amount of fault-enclosed compartments.

On the western rift margin, the main zones of low R_{22} (<0.01) are N-S striking, coinciding with the N-S-striking zones of high fault intensity and connecting node frequency (cf. Figure 8a with Figures 7a and 7b). The highest values of R_{22} are immediately adjacent to the North Viking Graben indicating that the western margin becomes more deformed with increasing distance from the North Viking Graben, this contrasts with the eastern margin. This is further supported by the map of fault-enclosed compartments, with negligible numbers or no compartments in areas adjacent to the North Viking Graben, except for the Gullfaks and Tampen Spur areas which are moderately compartmentalized. The smallest-sized compartments are clustered around the Magnus Sub-basin and the Tern-Eider Ridge, highlighting a relatively high amount of fault-enclosed compartments in these areas (Figure 8b).

4.3. Spatial Distribution of Strain, Faulting, and Topology

Table 2 summarizes values for the spatial heterogeneity of faulting (V_f') and fault throw (as a proxy for strain; V_s'), extracted from sampling along four across-strike transects, X, A, B, and C (see Figure 1b for locations and
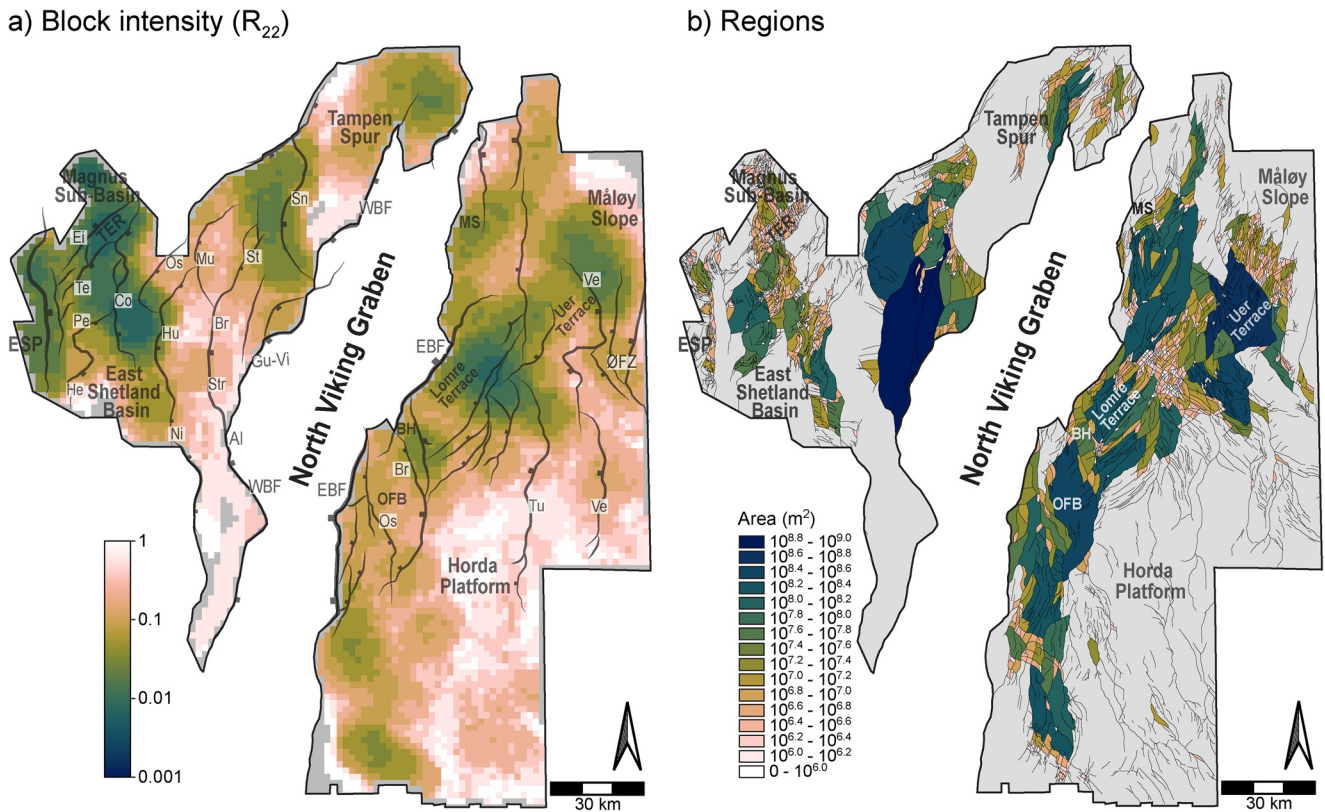
Figure 8. Spatial distribution of the rift margin compartmentalization. (a) Dimensionless block intensity (R_{22}) and (b) regions, showing how deformed or intact the margins are, and the fault-enclosed compartments, respectively. The major faults and structural elements are indicated for easy reference to locations. See Figure 1b for definition of abbreviations.

Figures S3–S6 in Supporting Information S1 for the seismic sections). The V_f' and V_s' values indicate how localized or distributed deformation is (Nixon, Bull, & Sanderson, 2014). To better understand controls on spatial variations and inter-relationship between fault network properties, we compare these values with variations in fault network geometry and topology along the transects.

4.3.1. Eastern Versus Western Rift Margin

Transect X runs across the entire rift and provides a comparison between the eastern and western rift margins (Figure 9). Cumulative throw and fault frequency plots along Transect X are presented in Figure 9a, illustrating the spatial distribution of strain and faulting. The eastern margin shows values of 0.24 and 0.28 for V_f' and V_s', respectively, indicating a low degree of heterogeneity of faulting and strain. Faulting on the western margin is also show low degree of heterogeneity, $V_f' = 0.28$, however strain is more localized with an elevated V_s' of 0.39, implying that a few faults accommodate most of the cumulative throw (Figure 9a, see also Table 2).

Table 2
Summary of the Heterogeneity Parameters of Faulting and Strain, V_f' and V_s'

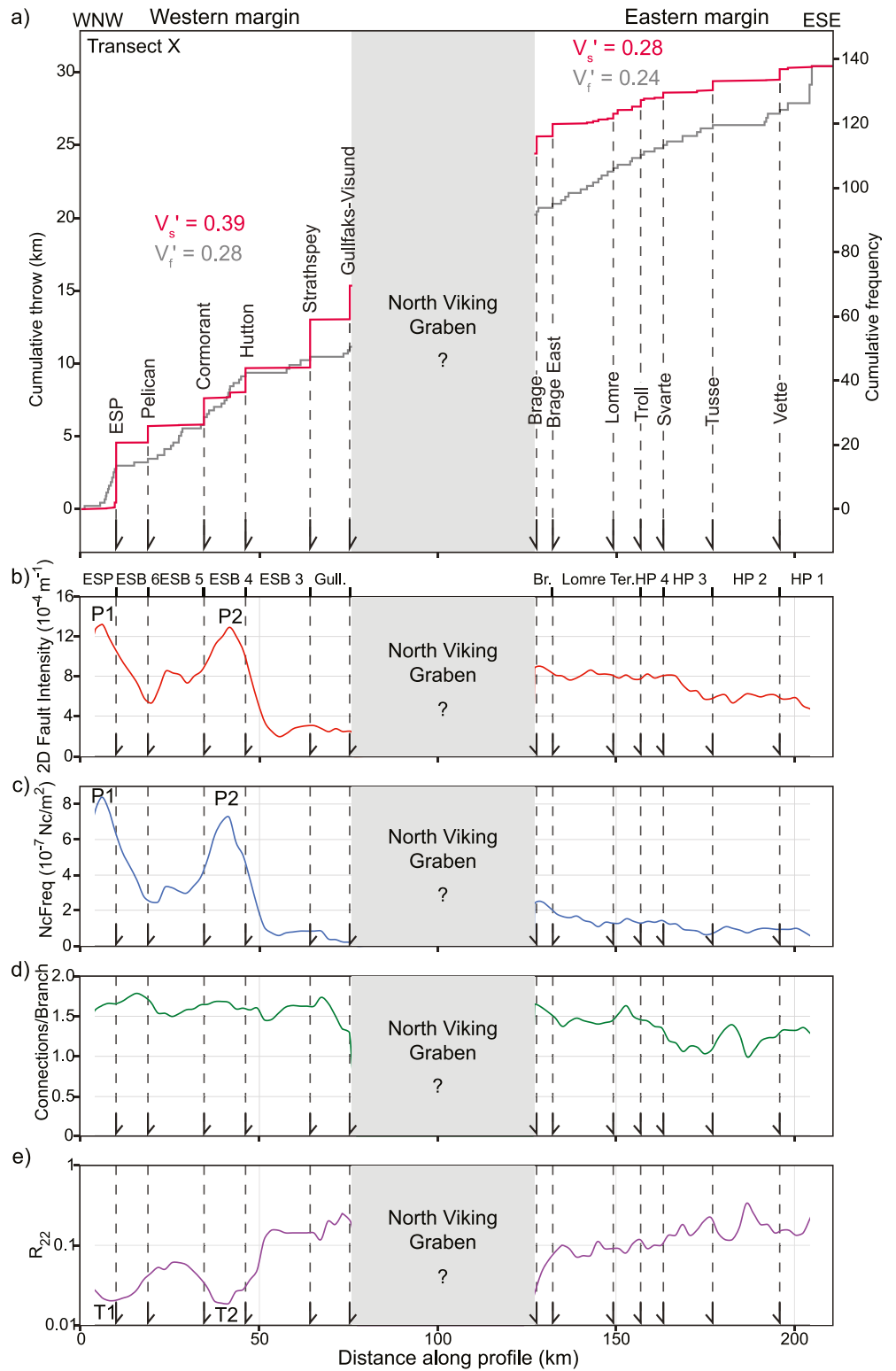| Transect	V_f'	V_s'
Regional transect X		
Eastern margin	0.24	0.28
Western margin	0.28	0.39
Horda Platform transects		
Transect A	0.37	0.36
Transect B	0.33	0.57
Transect C	0.43	0.54

Figure 9. (a) Cumulative plots of fault throw (solid red line) and fault frequency (solid gray line) for the across-strike, regional Transect X (see Figure 1b for location of the transect), with the corresponding, (b) 2D fault intensity plot, (c) connecting node frequency plot, (d) connections per branch plot, (e) block intensity plot, measured from the contour map in Figures 7 and 8a. Note that cumulative frequency and throw across the North Viking Graben were extrapolated from the margins.

Along the eastern rift margin, the fault intensity and connecting node frequency gradually decrease away from the North Viking Graben (Figures 9b and 9c). However, on the western rift margin the fault intensity and connecting node frequency decrease toward the North Viking Graben and exhibit two significant peaks, P1 and P2, indicating areas of localized high fault intensities (Figures 9b and 9c). P1 is located in the immediate footwall of the high-displacement, east-dipping, East Shetland Platform Fault, whereas P2 is located between the Cormorant and Hutton Fault zones in the East Shetland Basin 4 fault block. Values of C_B are slightly lower on the eastern rift margin compared to the western rift margin (Figure 9d). On the eastern rift margin, C_B correlates with fault intensity and connecting node frequency, decreasing away from the North Viking Graben. However, values for C_B are relatively constant on the western margin, and do not follow the localized variations in fault intensity and connecting node frequency (i.e., P1 and P2). The dimensionless block intensity (R_{22}) has an inverse relationship with fault intensity and connecting node frequency (Figure 9e). On the eastern margin, R_{22} increases steadily away from the North Viking Graben (Figure 9e). On the western margin, R_{22} is characterized by two major troughs, T1 (at the footwall of the East Shetland Platform Fault) and T2 (located between the Cormorant and Hutton Fault zones) that corresponds to peaks P1 and P2, respectively, and indicates two localized areas where the margin is highly deformed into numerous fault-enclosed compartments (compare Figure 9e with Figures 9b and 9c).

4.3.2. Along-Strike Spatial Variation in Strain and Fault Network Properties

Transects A, B, and C along the Horda Platform illustrate along-strike variations between different network properties and their relationship with strain. Transect A runs across the northern Horda Platform and through Lomre Terrace, Transect B runs across the central part of the Horda Platfrom and through the Oseberg Fault Block, and Transect C runs along the southern Horda Platform (Figure 1b). The spatial heterogeneity of faulting shows a homogenous distribution of faulting on the northern ($V'_f = 0.37$) and central ($V'_f = 0.33$) Horda Platform and a more heterogenous distribution of faulting on the southern Horda Platfrom ($V'_f = 0.43$) (Figure 10a–10c). Fault throw is also homogenously distributed on the northern Horda Platform, with a low V'_s of 0.36 indicating that strain is more distributed, being accommodated by both major faults and numerous smaller faults (Figure 10a). In contrast, throw is much more heterogeneous on the central and southern Horda Platform ($V'_s > 0.5$), indicating that strain is localized on to a few major faults, and is consistent with the cumulative throw plot, where it is mainly the major faults that contributes to the overall strain along the respective transects (Figures 10b and 10c).

The spatial patterns of fault intensity, connecting node frequency, C_B, and R_{22} show along-strike spatial variability of the fault network properties from the north to south of Horda Platform (Figures 10d–10o). The fault network properties generally decrease (or increase in the case of R_{22}) away from the North Viking Graben into the Horda Platform along all three transects (Figures 10d–10o). In general, the fault network properties show less variation along the northern Horda Platform transect, compared to the central and southern Horda Platform where they are characterized by several peaks and troughs (Figures 10d–10o). The peaks and troughs on the central and southern Horda Platform transects is consistent with the heterogenous throw (high V'_s values) representing localized strain.

The fault intensity, connecting node frequency, and C_B plots along the northern Horda Platform transect show an initial increase up to a maximum peak that coincides with the location of the Lomre-Troll fault system, followed by a gradual decrease farther eastwards into the Horda Platform (Figures 10d, 10g, and 10j). The R_{22} plot shows an inverse relationship to the other network properties (Figure 10m). Compared to the northern Horda Platform, the fault network properties on the central Horda Platform transect are characterized by several peaks and troughs, suggesting areas of localized high fault intensity, connectivity, and margin deformation (Figures 10e, 10h, 10k, and 10n). The peaks and troughs coincide with the immediate footwall of the Eastern Border Fault of the North Viking Graben, the Brage fault, and the Vette fault. The patterns of the fault network properties along the southern Horda Platform transect are identical to the central Horda Platform, specifically up to c. 70 km of the central transect (e.g., compare Figures 10i and 10h). An initial peak and trough for R_{22} that coincides with the immediate footwall of the Eastern Border Fault of the North Viking Graben is also recognized (Figures 10f, 10i, 10l, and 10o).

5. Discussion

5.1. Topological Characterization of Rift Structural Domains

Different structural domains reflect the rift-scale architecture of extensional rift or graben systems (Fossen et al., 2000; Gabrielsen, 1986; Nøttvedt et al., 1995; Robson, 1971). Gabrielsen (1986) presented an idealized
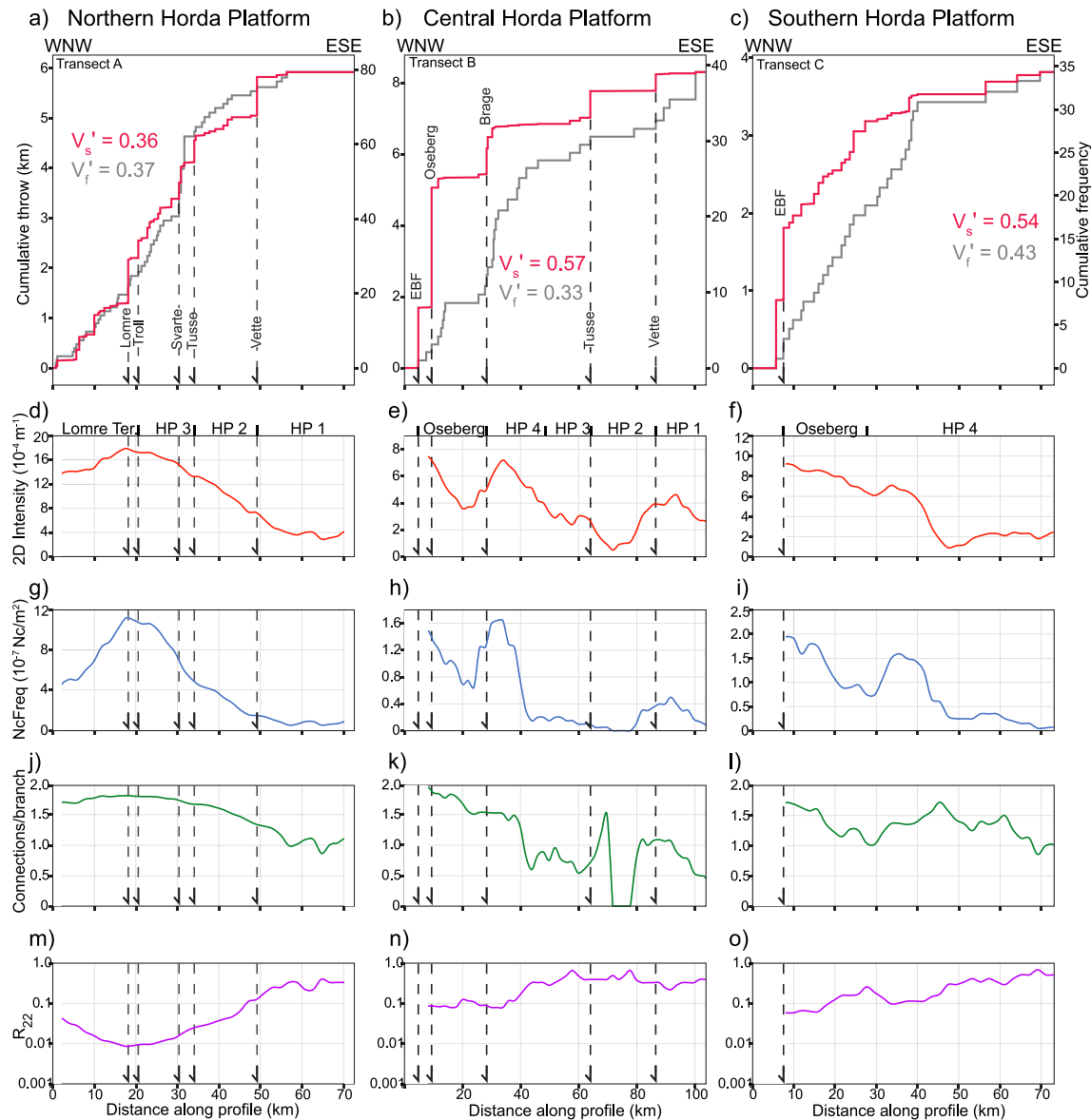
Figure 10. Cumulative plots of fault throw (solid red lines) and fault frequency (solid gray lines) for (a) Transect A, (b) Transect B, (c) Transect C, along the northern-, central-, and southern- Horda Platform, respectively (see Figure 1b for location of the transects). (d–f) 2D fault intensity plots corresponding to the transects. (g–i) Connecting node frequency plots corresponding to the transects. (j–l) Connections per branch plots corresponding to the transects. (m–o) Block intensity plots corresponding to the transects.

classification of the structural domains of a mature graben system based on observations of the fault geometries and degree of subsidence across and along the northern North Sea rift system. According to Gabrielsen's (1986) classification, the rift zone is separated from its undeformed surroundings by marginal fault complexes, and the architecture of the rift system can be subdivided mainly into: platform, sub-platform, and interior graben. The sub-platform typically consists of terraces and sub-basins.

In this study, the analysis of the topological properties of the fault network of the northern North Sea rift system, broadens the traditional approach of fault networks analysis, that is largely based on their geometry and kinematics (e.g., Bell et al., 2014; Claringbould et al., 2017; Deng et al., 2017; Osagiede et al., 2020). We present, for the first time, a detailed analysis of the spatial variation of the geometry (fault orientation and intensity), topology (network connectivity and compartmentalization), and strain (strain heterogeneity) of normal fault network at the rift-scale (up to several 1,000 s of km^2).
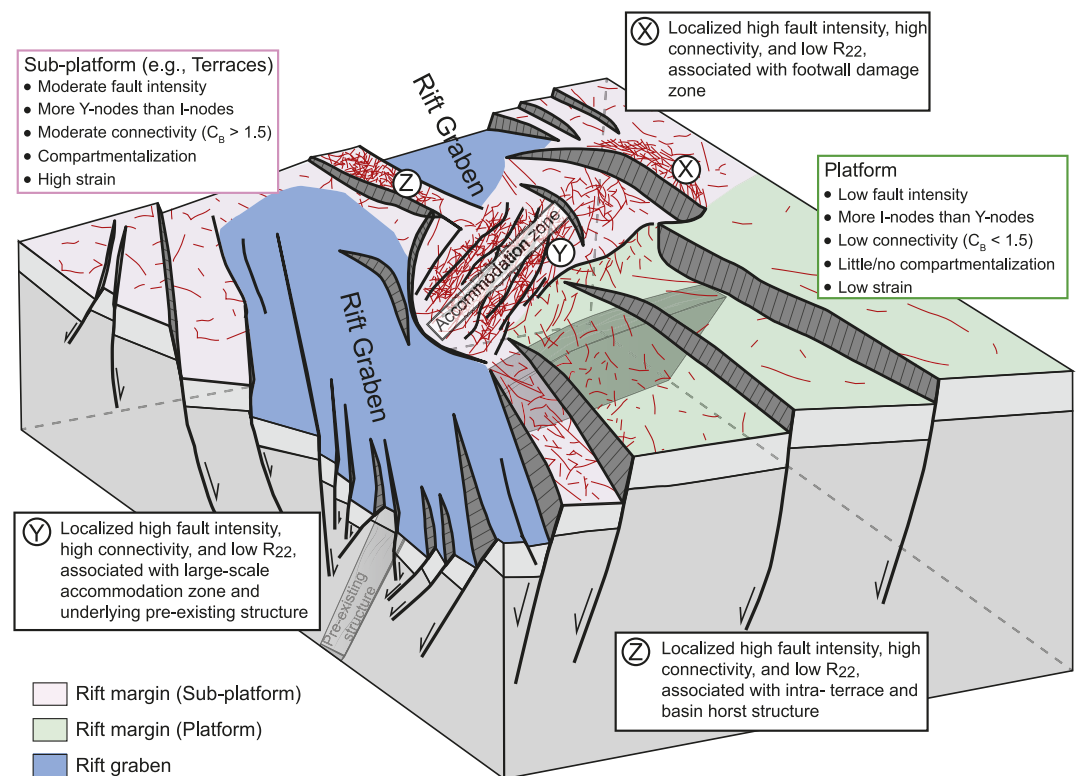
Figure 11. Summary of the key characteristics of the northern North Sea rift fault network in relation to the structural architecture (platform vs. sub-platform) of the rift margin. Local structurally complex areas X, Y, and Z, of high fault intensity, connectivity, host rock damage, and fault-enclosed compartmentalization are associated with footwall damage zone, rift accommodation zone, and intra-basin high/horst structure, respectively. Note the correlation between the location and orientation of the underlying pre-existing basement structure and the location and orientation of the accommodation zone faults.

The orientation of the faults within the fault network varies spatially between the rift margin fault blocks (see Figures 4 and 5). The dominant orientations of the faults within fault blocks that are adjacent to the North Viking Graben are sub-parallel to the graben axis, consisting of either N-S- or NE-SW- striking faults that may have been controlled by the graben border fault system. There is less influence of the graben border fault system on the fault orientations within fault blocks that are farther away from the North Viking Graben, where c. NW-SE orientations become dominant. Variations in the orientation of faults in different parts of the northern North Sea rift has also been recognized by several previous studies (e.g., Bartholomew et al., 1993; Claringbould et al., 2017; Færseth et al., 1997; Fossen et al., 2003; Osagiede et al., 2020; Reeve et al., 2015; Wrona et al., 2022). The topology of the rift is dominated by I-C- and C-C-branches, and I- and Y-nodes rather than X-nodes (Figure 6; Table 1), suggesting that the overall rift fault network is characterized by more isolated and abutting and/or splaying faults, and less cross-cutting faults. Similar observations of the dominance of I- or Y-nodes compared to X-nodes have been made in other rift fault networks in, for example, the Gulf of Thailand (Morley & Nixon, 2016), the Gulf of Suez (Duffy et al., 2017), and the Milne Point, Alaska North Slope (Duffy et al., 2017). This relatively low proportion of X-nodes within the fault network is likely related to the difficulty of preserving cross-cutting intersections as rift faults accumulate higher displacement, but may also have been impacted by the scale of observation, that is, the limited resolution of seismic data (e.g., Nixon et al., 2012).

The rift-scale analysis of the node and branch topology has also revealed two topological domains, one of which consists of fault blocks dominated by I-nodes and connections per branch (C_B) values <1.5, whereas the other consist of fault blocks dominated by Y-nodes and C_B values >1.5 (Figure 6; Table 1). Overall, these topological domains distinguish the fault blocks of the platform area (Horda Platform) from those of the sub-platform areas (e.g., Lomre Terrace and East Shetland Basin) in the northern North Sea (Figure 6). This suggests that the platform area of the rift margin is characterized by a relatively simple network dominated by isolated faults, and low connectivity, whereas the sub-platform area is characterized by a more complex network dominated by abutting

and/or splaying faults, and moderate connectivity (Figure 11). This topological domain subdivision of the rift margin is further supported by the results of the contour grid sampling that show the spatial variability of rift fault network properties (Figures 7 and 8). The rift fault network properties, that is, the fault intensity, connecting node frequency, and C_B are generally lower and block intensity is higher on the platform area (e.g., the Horda Platform) compared to the sub-platform area (e.g., Lomre Terrace and East Shetland Basin; see Figures 7 and 8). The platform area of rift margins is interpreted to be less faulted and less deformed (or more intact), and the rift fault network is less connected and less compartmentalized in comparison to the sub-platform area (Figure 11). The inclusion of the topological analysis of the rift fault network in this interpretation therefore provides a new, complimentary way to characterize the large-scale structural domains in rifts.

Previous studies have shown that within rift margins, the platform areas exhibit relatively moderate internal faulting and accommodate moderate subsidence, whereas the sub-platform area have more closely spaced internal faults and accommodate higher amounts of subsidence (e.g., Fossen et al., 2000; Gabrielsen, 1986; Nøttvedt et al., 1995). An important question then is, what controls the topological domains of rift margins at rift-scale? We suggest that the observed distinct topological characteristics of the platform and sub-platform structural domains reflect the amount of strain accommodated within the structural domains. This conclusion agrees with that of Duffy et al. (2017), based on their investigation of how the node and branch topology evolved with increasing strain on a set of clay experimental models. Their results showed that I-nodes and I-C branches dominate the fault network topology at relatively low strain, whereas Y-nodes and C-C-branches dominate under high strain, which is similar to our observations of the topology of the platform and sub-platform, respectively.

5.2. Local Controls on the Spatial Variability of the Rift Fault Network Properties

Although we suggest that the overall topological patterns that characterize the rift structural domains is controlled by the relative amount of strain accommodated within the domains, there are, however, local variations in the properties of the rift fault network that are possibly linked to other factors, which we discuss here.

5.2.1. Role of Pre-Existing Structures and Accommodation Zone

Several pre-existing shear zones related to the post-orogenic extensional collapse of the Caledonian orogen are interpreted within the crustal basement that underlie the northern North Sea rift (e.g., Fazlikhani et al., 2017; Phillips et al., 2019; Osagiede et al., 2020; Figure 1a). One of the most prominent of these shear zones in the study area is the NE-SW striking Lomre Shear Zone which underlies the Lomre Terrace (Figure 1a). Based on our observation, rift faults within the Lomre Terrace fault block have a dominant NE-SW strike, suggesting that the underlying Lomre Shear Zone may have locally influenced the orientation of the faults. This interpretation agrees with previous conclusion by Tillmans (2020). Also, the location of the Lomre Shear Zone coincides with rift accommodation zone, associated with a right-step of the graben axis between the North Viking- and Sogn-graben rift segments. This suggests that the Lomre Shear Zone may not have only influenced the orientation of the cover rift faults in its immediate vicinity, but also the larger-scale rift architecture through its influence on the location of the North Viking–Sogn graben rift accommodation zone.

The structural complexity of the rift accommodation zone around the Lomre Terrace is reflected in the topology of the rift fault network. The area is one of the areas characterized by localized high fault intensity, high connectivity ($C_B > 1.7$), intense margin deformation ($R_{22} < 0.1$), and relatively high amount of fault-enclosed compartments (Figures 7 and 8). Also, a clear NE-SW-striking zone of high fault intensity and connecting node frequency along the Lomre–Uer terraces mimic the orientation of the underlying Lomre Shear Zone (see Figures 7a and 7b). Furthermore, the along-strike spatial heterogeneity analysis of faulting and strain revealed that deformation is distributed (increased faulting and complexity) around the rift accommodation zone. We therefore argue that the presence of the underlying pre-existing structure and the associated rift accommodation zone locally influenced the observed spatial variation of the geometry, strain heterogeneity, and topology of the rift margin fault network (Figure 11).

5.2.2. Influence of Fault Damage and Intra-Basin Highs on Rift Fault Network Properties

Several localized structurally complex areas of high fault intensity, high connectivity ($C_B > 1.7$), intense deformation ($R_{22} < 0.1$) and high amount of fault-enclosed compartments, coincides with the immediate footwall of some of the major, high-displacement faults. Examples of intense footwall deformation include the northern segment of the Vette fault on the eastern rift margin, and the Snorre and Cormorant faults on the western rift margin (Figures 7 and 8).

We suggest that this relationship is related to a high degree of deformation associated with wall damage as a result of repeated accumulation of slip on the major faults over time (Cowie & Scholz, 1992; Kim et al., 2004; Vermilye & Scholz, 1998). This suggestion is consistent with other recent studies where similar observation of increased fault abundance and connectivity in fault damage zones have been documented (e.g., Hansberry et al., 2021; Nixon et al., 2020). For example, Hansberry et al. (2021) used node and branch topology to distinguish damage zone fracturing from background fracturing in the hanging-wall of the Castle Cove Fault, Otway Basin. They showed that the intensity and connectivity of fractures significantly increased in the immediate hanging-wall of the fault, whereas the background fracturing remained relatively unchanged, providing a basis to quantify the width of the damage zone.

Other local structurally complex areas are related with fault-bounded horst blocks that form intra-basin highs, for example, the Marflo Spur and Brage Horst on the eastern rift margin, and the Tern-Eider Ridge on the western rift margin (Figures 7 and 8). Although it is not exactly clear why the horst blocks are intensely deformed, we speculate that the observed intense deformation may be related to an overlapping of the footwall damage zones associated with the major faults that bounds the horsts. The correlation between the location of local structurally complex areas within the rift fault network and either fault damage zones or intra-basin highs suggest that the development of both fault damage zones and intra-basin highs can also influence the spatial variability of rift fault networks properties (Figure 11).

5.3. Relationship Between Rift Fault Network Geometry, Topology, and Strain Heterogeneity

Our results also provide insights on the relationship between different fault network properties that are related to the geometry, topology, and strain distribution within rift. Based on the results of the contour grid sampling, all the rift fault network properties (except C_B) exhibit near-identical patterns of spatial variability (Figures 7 and 8). In general, where the fault intensity is high, for example, around the Lomre Terrace in the eastern rift margin and Tern-Eider Ridge in the western rift margin, the corresponding connecting node frequency and C_B are also high, whereas the dimensionless block intensity (R_{22}) is low, and the identified regions are characterized by numerous small-sized fault-enclosed compartments (Figures 7 and 8). On the other hand, where the fault intensity is low, for example, around the Horda Platform, the corresponding connecting node frequency and C_B are also low, whereas R_{22} is high, and little or no regions (fault-enclosed compartments) are identified (Figures 7 and 8). These correlations between the rift fault network properties suggest that the geometry (i.e., orientation and intensity) and topology (i.e., connectivity and compartmentalization) of the network are inter-related at rift-scale. Similar relationship, where the combination of the variability in orientation and abundance of faults or fractures dictate the degree of connectivity and relative amount of compartmentalization have been recognized in rift fault networks (Duffy et al., 2017; Morley & Nixon, 2016) and fracture networks in general (e.g., Dimmen et al., 2020; Nixon et al., 2020; Sanderson & Nixon, 2018), at both outcrop- and basin-scale. The similarity in the highlighted relationship between rift fault network geometry and topology at different scales suggest that this relationship may be applicable irrespective of the scale of observation.

The regional transect across the eastern and western margins of the northern North Sea rift show variability of the heterogeneity parameters for faulting (V_f') and strain (V_s') across the rift (Figure 9a). Values of both V_f' and V_s' are lower on the eastern rift margin compared to the western margin, indicating that the eastern rift margin has distributed faulting and strain, whereas faulting and strain are more localized on the western rift margin. The distributed and localized faulting and strain observed in the eastern and western rift margin, respectively, also directly reflect on other fault network properties like the fault intensity, connecting node frequency and R_{22}, plotted along the transect (Figure 9). The values of these properties on the eastern rift margin of the transect are less variable, decreasing gradually away from the North Viking Graben, in line with distributed faulting and strain, whereas on the western margin, the properties are more variable, exhibiting local peaks and troughs due to localized faulting and strain (Figure 9). This suggests that changes in throw accommodated by major faults and strain localization also imposes a first order control on fault network geometry and topology.

6. Conclusions

We have assessed the geometry, topology, and strain heterogeneity of the northern North Sea rift margin fault network, using variance surface attribute extracted from high quality 3D seismic reflection data. Our results

provide a new way to characterize large-scale rift structural domains and shed light on controls on the spatial variability of network properties such as intensity, connectivity, and compartmentalization within rift fault networks. The key findings are summarized as follows:

1. Fault orientation varies spatially within the rift margin, exhibiting predominantly N-S, NE-SW, and NW-SE strikes. The variation is related to proximity to the border fault system of the North Viking Graben, the step (accommodation zone) in the rift, and presence of underlying pre-existing structures.
2. The overall topology of the rift margin fault network is I- and Y- nodes, and I-C- and C-C- branches dominated, with X-nodes rarely preserved.
3. The rift topology varies spatially, which at rift-scale is related to the broad structural domains of the rift margin, that is, platform versus sub-platform consisting of terraces and basins. The platform area is characterized by low fault intensity and connectivity, and it is less deformed with little or no fault-enclosed compartments, whereas the sub-platform area is characterized by moderate fault intensity and connectivity, more deformed and highly compartmentalized.
4. The difference in the topology of the platform versus sub-platform structural domains is controlled by the relatively low strain accommodated in platform area, compared to high strain in the sub-platform area.
5. Several other factors including the presence of pre-existing basement structure, rift segment interaction (accommodation) zone, fault damage zone, and intra-basin highs locally influence the geometry, topology and strain distribution of the rift. They result in the development of localized structurally complex areas of high fault intensity, high connectivity, intense margin deformation and compartmentalization.
6. The topology of rift fault network is to a great extent related to and dependent on the geometry and strain distribution of the network, irrespective of the scale of observation.

Data Availability Statement

The 3D reflection seismic data underlying this study is a property of CGG and may be accessed by formally writing to CGG. However, with permission from CGG, we have made some seismic sections available in Supporting Information S1. The NetworkGT software developed by Nyberg et al. (2018) and used for topological analysis in this study is available open access at https://github.com/BjornNyberg/NetworkGT.

References

Aydin, A. (2000). Fractures, faults, and hydrocarbon entrapment, migration and flow. *Marine and Petroleum Geology*, *17*(7), 797–814. https://doi.org/10.1016/s0264-8172(00)00020-9

Badley, M., Price, J., Dahl, C. R., & Agdestein, T. (1988). The structural evolution of the northern Viking Graben and its bearing upon extensional modes of basin formation. *Journal of the Geological Society*, *145*(3), 455–472. https://doi.org/10.1144/gsjgs.145.3.0455

Bartholomew, I., Peters, J., & Powell, C. (1993). Regional structural evolution of the North Sea: Oblique slip and the reactivation of basement lineaments. In *Paper presented at the geological society, London, petroleum geology conference series*.

Bell, R. E., Jackson, C. A. L., Whipp, P. S., & Clements, B. (2014). Strain migration during multiphase extension: Observations from the northern North Sea. *Tectonics*, *33*(10), 1936–1963. https://doi.org/10.1002/2014tc003551

Bell, R. E., McNeill, L., Bull, J., Henstock, T., Collier, R. L., & Leeder, M. (2009). Fault architecture, basin structure and evolution of the Gulf of Corinth Rift, central Greece. *Basin Research*, *21*(6), 824–855. https://doi.org/10.1111/j.1365-2117.2009.00401.x

Cartwright, J. A., Trudgill, B. D., & Mansfield, C. S. (1995). Fault growth by segment linkage: An explanation for scatter in maximum displacement and trace length data from the Canyonlands Grabens of SE Utah. *Journal of Structural Geology*, *17*(9), 1319–1326. https://doi.org/10.1016/0191-8141(95)00033-a

Chopra, S., & Marfurt, K. J. (2005). Seismic attributes—A historical perspective. *Geophysics*, *70*(5), 3SO–28SO. https://doi.org/10.1190/1.2098670

Claringbould, J. S., Bell, R. E., Jackson, C. A.-L., Gawthorpe, R. L., & Odinsen, T. (2017). Pre-existing normal faults have limited control on the rift geometry of the northern North Sea. *Earth and Planetary Science Letters*, *475*, 190–206. https://doi.org/10.1016/j.epsl.2017.07.014

Coward, M., Dewey, J., Hempton, M., & Holroyd, J. (2003). Tectonic evolution. In D. Evans, C. Graham, A. Armour, & P. Bathurst (Eds.), *The millennium Atlas: Petroleum geology of the central and northern North Sea* (pp. 17–33). The Geological Society of London.

Cowie, P. A., & Scholz, C. H. (1992). Growth of faults by accumulation of seismic slip. *Journal of Geophysical Research*, *97*(B7), 11085–11095. https://doi.org/10.1029/92jb00586

Daly, M., Chorowicz, J., & Fairhead, J. (1989). Rift basin evolution in Africa: The influence of reactivated steep basement shear zones. *Geological Society, London, Special Publications*, *44*(1), 309–334. https://doi.org/10.1144/gsl.sp.1989.044.01.17

Davies, R., O'donnell, D., Bentham, P., Gibson, J., Curry, M., Dunay, R., & Maynard, J. (1999). The origin and genesis of major Jurassic unconformities within the triple junction area of the North Sea, UK. In *Paper presented at the geological society, London, petroleum geology conference series*.

Deng, C., Fossen, H., Gawthorpe, R. L., Rotevatn, A., Jackson, C. A., & FazliKhani, H. (2017). Influence of fault reactivation during multiphase rifting: The Oseberg area, Northern North Sea rift. *Marine and Petroleum Geology*, *86*, 1252–1272. https://doi.org/10.1016/j.marpetgeo.2017.07.025

Dershowitz, W., & Einstein, H. (1988). Characterizing rock joint geometry with joint system models. *Rock Mechanics and Rock Engineering*, *21*(1), 21–51. https://doi.org/10.1007/bf01019674

Dewey, J. F. (1988). Extensional collapse of orogens. *Tectonics*, *7*(6), 1123–1139. https://doi.org/10.1029/tc007i006p01123

Dimmen, V., Rotevatn, A., & Nixon, C. W. (2020). The relationship between fluid flow, structures, and depositional architecture in sedimentary rocks: An example-based overview. *Geofluids*, *2020*, 1–19. https://doi.org/10.1155/2020/3506743

Dimmen, V., Rotevatn, A., Peacock, D. C., Nixon, C. W., & Nærland, K. (2017). Quantifying structural controls on fluid flow: Insights from carbonate-hosted fault damage zones on the Maltese Islands. *Journal of Structural Geology*, *101*, 43–57. https://doi.org/10.1016/j.jsg.2017.05.012

Dreyer, T., Whitaker, M., Dexter, J., Flesche, H., & Larsen, E. (2005). From spit system to tide-dominated delta: Integrated reservoir model of the upper Jurassic Sognefjord formation on the troll west field. In *Paper presented at the geological society, London, petroleum geology conference series*.

Duffy, O. B., Bell, R. E., Jackson, C. A. L., Gawthorpe, R. L., & Whipp, P. S. (2015). Fault growth and interactions in a multiphase rift fault network: Horda Platform, Norwegian North Sea. *Journal of Structural Geology*, *80*, 99–119. https://doi.org/10.1016/j.jsg.2015.08.015

Duffy, O. B., Nixon, C. W., Bell, R. E., Jackson, C. A. L., Gawthorpe, R. L., Sanderson, D. J., & Whipp, P. S. (2017). The topology of evolving rift fault networks: Single-phase vs multi-phase rifts. *Journal of Structural Geology*, *96*, 192–202. https://doi.org/10.1016/j.jsg.2017.02.001

Dunbar, J. A., & Sawyer, D. S. (1988). Continental rifting at pre-existing lithospheric weaknesses. *Nature*, *333*(6172), 450–452. https://doi.org/10.1038/333450a0

Ebinger, C. J. (1989). Geometric and kinematic development of border faults and accommodation zones, Kivu-Rusizi rift, Africa. *Tectonics*, *8*(1), 117–133. https://doi.org/10.1029/tc008i001p00117

Espejel, R. L., Alves, T. M., & Blenkinsop, T. G. (2020). Multi-scale fracture network characterisation on carbonate platforms. *Journal of Structural Geology*, *140*, 104160. https://doi.org/10.1016/j.jsg.2020.104160

Færseth, R. (1996). Interaction of Permo-triassic and Jurassic extensional fault-blocks during the development of the northern North Sea. *Journal of the Geological Society*, *153*(6), 931–944. https://doi.org/10.1144/gsjgs.153.6.0931

Færseth, R., Knudsen, B., Liljedahl, T., Midbue, P., & Søderstrøm, B. (1997). Oblique rifting and sequential faulting in the Jurassic development of the northern North Sea. *Journal of Structural Geology*, *19*(10), 1285–1302. https://doi.org/10.1016/s0191-8141(97)00045-x

Færseth, R., & Ravnås, R. (1998). Evolution of the Oseberg fault-block in context of the northern North Sea structural framework. *Marine and Petroleum Geology*, *15*(5), 467–490. https://doi.org/10.1016/s0264-8172(97)00046-9

Fazlikhani, H., Fossen, H., Gawthorpe, R. L., Faleide, J., & Bell, R. E. (2017). Basement structure and its influence on the structural configuration of the northern North Sea.

Fossen, H. (1992). The role of extensional tectonics in the Caledonides of south Norway. *Journal of Structural Geology*, *14*(8), 1033–1046. https://doi.org/10.1016/0191-8141(92)90034-t

Fossen, H. (1998). Advances in understanding the post-Caledonian structural evolution of the Bergen area, West Norway. *Norsk Geologisk Tidsskrift*, *78*(1), 33–46.

Fossen, H. (2020). Fault classification, fault growth and displacement. In *Regional geology and tectonics: Principles of geologic analysis*.

Fossen, H., & Dunlap, W. J. (1999). On the age and tectonic significance of Permo-Triassic dikes in the Bergen-Sunnhordland region, southwestern Norway. *Norsk Geologisk Tidsskrift*, *79*(3), 169–178. https://doi.org/10.1080/002919699433807

Fossen, H., Hesthammer, J., Johansen, T. E. S., & Sygnabere, T. O. (2003). Structural geology of the Huldra field, northern North Sea—A major tilted fault block at the eastern edge of the Horda platform. *Marine and Petroleum Geology*, *20*(10), 1105–1118. https://doi.org/10.1016/j.marpetgeo.2003.07.003

Fossen, H., Khani, H. F., Faleide, J. I., Ksienzyk, A. K., & Dunlap, W. J. (2017). Post-caledonian extension in the West Norway–northern North Sea region: The role of structural inheritance. In C. Childs, R. E. Holdsworth, C. A.-L. Jackson, T. Manzocchi, J. J. Walsh, & G. Yielding (Eds.), *Geological society, London, special publications* (Vol. 439, pp. 465–486).

Fossen, H., Odinsen, T., Færseth, R. B., & Gabrielsen, R. H. (2000). *Detachments and low-angle faults in the northern North Sea rift system* (Vol. 167, pp. 105–132). Special Publication-Geological Society of London.

Gabrielsen, R. (1986). Structural elements in graben systems and their influence on hydrocarbon trap types. In *Paper presented at the Habitat of hydrocarbons on the Norwegian continental shelf. International conference*.

Gawthorpe, R. L., & Leeder, M. R. (2000). Tectono-sedimentary evolution of active extensional basins. *Basin Research*, *12*(3–4), 195–218. https://doi.org/10.1111/j.1365-2117.2000.00121.x

Gee, D. G., Fossen, H., Henriksen, N., & Higgins, A. K. (2008). From the early Paleozoic platforms of Baltica and Laurentia to the Caledonide Orogen of Scandinavia and Greenland. *Episodes*, *31*(1), 44–51. https://doi.org/10.18814/epiiugs/2008/v31i1/007

Gillespie, P., Howard, C., Walsh, J., & Watterson, J. (1993). Measurement and characterisation of spatial distributions of fractures. *Tectonophysics*, *226*(1–4), 113–141. https://doi.org/10.1016/0040-1951(93)90114-y

Glennie, K. W. (1986). The structural framework and the pre-Permian history of the North Sea area. In K. W. Glennie (Ed.), *Introduction to the petroleum geology of the North Sea* (2nd ed., pp. 25–62). Blackwell Scientific Publications.

Hansberry, R. L., King, R. C., Holford, S. P., Hand, M., & Debenham, N. (2021). How wide is a fault damage zone? Using network topology to examine how fault-damage zones overprint regional fracture networks. *Journal of Structural Geology*, *146*, 104327. https://doi.org/10.1016/j.jsg.2021.104327

Helland-Hansen, W., Ashton, M., Lømo, L., & Steel, R. (1992). Advance and retreat of the brent delta: Recent contributions to the depositional model. *Geological Society, London, Special Publications*, *61*(1), 109–127. https://doi.org/10.1144/gsl.sp.1992.061.01.07

Henza, A. A., Withjack, M. O., & Schlische, R. W. (2010). Normal-fault development during two phases of non-coaxial extension: An experimental study. *Journal of Structural Geology*, *32*(11), 1656–1667. https://doi.org/10.1016/j.jsg.2009.07.007

Henza, A. A., Withjack, M. O., & Schlische, R. W. (2011). How do the properties of a pre-existing normal-fault population influence fault development during a subsequent phase of extension? *Journal of Structural Geology*, *33*(9), 1312–1324. https://doi.org/10.1016/j.jsg.2011.06.010

Holgate, N. E., Jackson, C. A.-L., Hampson, G. J., & Dreyer, T. (2013). Sedimentology and sequence stratigraphy of the middle–upper jurassic krossfjord and fensfjord formations, Troll Field, northern North Sea. *Petroleum Geoscience*, *19*(3), 237–258. https://doi.org/10.1144/petgeo2012-039

Huseby, O., Thovert, J., & Adler, P. (1997). Geometry and topology of fracture systems. *Journal of Physics A: Mathematical and General*, *30*(5), 1415–1444. https://doi.org/10.1088/0305-4470/30/5/012

Jackson, C. A.-L., Grunhagen, H., Howell, J. A., Larsen, A. L., Andersson, A., Boen, F., & Groth, A. (2010). 3D seismic imaging of lower delta-plain beach ridges: Lower brent Group, northern North Sea. *Journal of the Geological Society*, *167*(6), 1225–1236. https://doi.org/10.1144/0016-76492010-053

Johnson, R., & Dingwall, R. (1981). The Caledonides: Their influence on the stratigraphy of the northwest European continental shelf. In *Petroleum geology of the continental shelf of North-West Europe*. Heyden.8597.

Jolley, S., Barr, D., Walsh, J., & Knipe, R. (2007). Structurally complex reservoirs: An introduction. *Geological Society, London, Special Publications*, *292*(1), 1–24. https://doi.org/10.1144/sp292.1

Jolley, S., Fisher, Q., & Ainsworth, R. (2010). Reservoir compartmentalization: An introduction. *Geological Society, London, Special Publications*, *347*(1), 1–8. https://doi.org/10.1144/sp347.1

Kim, Y.-S., Peacock, D. C., & Sanderson, D. J. (2004). Fault damage zones. *Journal of Structural Geology*, *26*(3), 503–517. https://doi.org/10.1016/j.jsg.2003.08.002

Ksienzyk, A. K., Jacobs, J., Fossen, H., Dunkl, I., & Kosler, J. (2013). The basement of the Utsira high: U/Pb, (U-Th)/He and fission track thermochronology. In *Paper presented at the Vinterkonferansen, Oslo.*

Lervik, K. (2006). Triassic lithostratigraphy of the northern North Sea basin. *Norsk Geologisk Tidsskrift*, *86*(2), 93.

Leveille, G. P., Knipe, R., More, C., Ellis, D., Dudley, G., Jones, G., et al. (1997). Compartmentalization of Rotliegendes gas reservoirs by sealing faults, Jupiter Fields area, southern North Sea. *Geological Society, London, Special Publications*, *123*(1), 87–104. https://doi.org/10.1144/gsl.sp.1997.123.01.06

Mansfield, C., & Cartwright, J. (1996). High resolution fault displacement mapping from three-dimensional seismic data: Evidence for dip linkage during fault growth. *Journal of Structural Geology*, *18*(2–3), 249–263. https://doi.org/10.1016/s0191-8141(96)80048-4

Manzocchi, T. (2002). The connectivity of two-dimensional networks of spatially correlated fractures. *Water Resources Research*, *38*(9), 1-1–1-20. https://doi.org/10.1029/2000wr000180

McKerrow, W., Mac Niocaill, C., & Dewey, J. (2000). The Caledonian orogeny redefined. *Journal of the Geological Society*, *157*(6), 1149–1154. https://doi.org/10.1144/jgs.157.6.1149

Meyer, V., Nicol, A., Childs, C., Walsh, J., & Watterson, J. (2002). Progressive localisation of strain during the evolution of a normal fault population. *Journal of Structural Geology*, *24*(8), 1215–1231. https://doi.org/10.1016/s0191-8141(01)00104-3

Mitchener, B., Lawrence, D., Partington, M., Bowman, M., & Gluyas, J. (1992). Brent Group: Sequence stratigraphy and regional implications. *Geological Society, London, Special Publications*, *61*(1), 45–80. https://doi.org/10.1144/gsl.sp.1992.061.01.05

Morley, C. K. (2017). The impact of multiple extension events, stress rotation and inherited fabrics on normal fault geometries and evolution in the Cenozoic rift basins of Thailand. *Geological Society, London, Special Publications*, *439*(1), 413–445. https://doi.org/10.1144/sp439.3

Morley, C. K., Gabdi, S., & Seusutthiya, K. (2007). Fault superimposition and linkage resulting from stress changes during rifting: Examples from 3D seismic data, Phitsanulok Basin, Thailand. *Journal of Structural Geology*, *29*(4), 646–663. https://doi.org/10.1016/j.jsg.2006.11.005

Morley, C. K., & Nixon, C. W. (2016). Topological characteristics of simple and complex normal fault networks. *Journal of Structural Geology*, *84*, 68–84. https://doi.org/10.1016/j.jsg.2016.01.005

Mulrooney, M. J., Osmond, J. L., Skurtveit, E., Faleide, J. I., & Braathen, A. (2020). Structural analysis of the Smeaheia fault block, a potential CO_2 storage site, northern Horda Platform, North Sea. *Marine and Petroleum Geology*, *121*, 104598. https://doi.org/10.1016/j.marpetgeo.2020.104598

Nicol, A., Walsh, J., Villamor, P., Seebeck, H., & Berryman, K. (2010). Normal fault interactions, paleoearthquakes and growth in an active rift. *Journal of Structural Geology*, *32*(8), 1101–1113. https://doi.org/10.1016/j.jsg.2010.06.018

Nixon, C. W., Bull, J. M., & Sanderson, D. J. (2014). Localized vs distributed deformation associated with the linkage history of an active normal fault, Whakatane Graben, New Zealand. *Journal of Structural Geology*, *69*, 266–280. https://doi.org/10.1016/j.jsg.2014.06.005

Nixon, C. W., Nærland, K., Rotevatn, A., Dimmen, V., Sanderson, D. J., & Kristensen, T. B. (2020). Connectivity and network development of carbonate-hosted fault damage zones from western Malta. *Journal of Structural Geology*, *141*, 104212. https://doi.org/10.1016/j.jsg.2020.104212

Nixon, C. W., Sanderson, D. J., & Bull, J. M. (2012). Analysis of a strike-slip fault network using high resolution multibeam bathymetry, offshore NW Devon UK. *Tectonophysics*, *541*, 69–80. https://doi.org/10.1016/j.tecto.2012.03.021

Nixon, C. W., Sanderson, D. J., Dee, S. J., Bull, J. M., Humphreys, R. J., & Swanson, M. H. (2014). Fault interactions and reactivation within a normal-fault network at Milne Point, Alaska. *AAPG Bulletin*, *98*(10), 2081–2107. https://doi.org/10.1306/04301413177

Nøttvedt, A., Gabrielsen, R., & Steel, R. (1995). Tectonostratigraphy and sedimentary architecture of rift basins, with reference to the northern North Sea. *Marine and Petroleum Geology*, *12*(8), 881–901. https://doi.org/10.1016/0264-8172(95)98853-w

Nyberg, B., Nixon, C. W., & Sanderson, D. J. (2018). NetworkGT: A GIS tool for geometric and topological analysis of two-dimensional fracture networks. *Geosphere*, *14*(4), 1618–1634. https://doi.org/10.1130/ges01595.1

Odinsen, T., Reemst, P., Van Der Beek, P., Faleide, J. I., & Gabrielsen, R. H. (2000). Permo-triassic and Jurassic extension in the northern North Sea: Results from tectonostratigraphic forward modelling. *Geological Society, London, Special Publications*, *167*(1), 83–103. https://doi.org/10.1144/gsl.sp.2000.167.01.05

Ogata, K., Senger, K., Braathen, A., & Tveranger, J. (2014). Fracture corridors as seal-bypass systems in siliciclastic reservoir-cap rock successions: Field-based insights from the Jurassic Entrada Formation (SE Utah, USA). *Journal of Structural Geology*, *66*, 162–187. https://doi.org/10.1016/j.jsg.2014.05.005

Osagiede, E. E., Rosenau, M., Rotevatn, A., Gawthorpe, R., Jackson, C. A. L., & Rudolf, M. (2021). Influence of zones of pre-existing crustal weakness on strain localization and partitioning during rifting: Insights from analog modeling using high-resolution 3D digital image correlation. *Tectonics*, *40*(10), e2021TC006970. https://doi.org/10.1029/2021tc006970

Osagiede, E. E., Rotevatn, A., Gawthorpe, R., Kristensen, T. B., Jackson, C. A., & Marsh, N. (2020). Pre-existing intra-basement shear zones influence growth and geometry of non-colinear normal faults, western Utsira High–Heimdal Terrace, North Sea. *Journal of Structural Geology*, *130*, 103908. https://doi.org/10.1016/j.jsg.2019.103908

Patruno, S., Hampson, G. J., Jackson, C. A. L., & Dreyer, T. (2015). Clinoform geometry, geomorphology, facies character and stratigraphic architecture of a sand-rich subaqueous delta: Jurassic Sognefjord Formation, offshore Norway. *Sedimentology*, *62*(1), 350–388. https://doi.org/10.1111/sed.12153

Peacock, D., Nixon, C., Rotevatn, A., Sanderson, D., & Zuluaga, L. (2016). Glossary of fault and other fracture networks. *Journal of Structural Geology*, *92*, 12–29. https://doi.org/10.1016/j.jsg.2016.09.008

Peacock, D., Nixon, C., Rotevatn, A., Sanderson, D., & Zuluaga, L. (2017). Interacting faults. *Journal of Structural Geology*, *97*, 1–22. https://doi.org/10.1016/j.jsg.2017.02.008

Phillips, T. B., Fazlikhani, H., Gawthorpe, R. L., Fossen, H., Jackson, C. A. L., Bell, R. E., et al. (2019). The influence of structural inheritance and multiphase extension on rift development, the northern North Sea. *Tectonics*, *38*(12), 4099–4126. https://doi.org/10.1029/2019tc005756

Phillips, T. B., Jackson, C. A. L., Bell, R. E., Duffy, O. B., & Fossen, H. (2016). Reactivation of intrabasement structures during rifting: A case study from offshore southern Norway. *Journal of Structural Geology*, *91*, 54–73. https://doi.org/10.1016/j.jsg.2016.08.008

Pickering, G., Peacock, D. C., & Lee, J. (1997). Modeling tip zones to predict the throw and length characteristics of faults. *AAPG Bulletin*, *81*(1), 82–99.

Platt, N. H. (1995). Structure and tectonics of the northern North Sea: New insights from deep penetration regional seismic data. *Geological Society, London, Special Publications*, *80*(1), 103–113. https://doi.org/10.1144/gsl.sp.1995.080.01.05

Putz-Perrier, M. W., & Sanderson, D. J. (2008). Spatial distribution of brittle strain in layered sequences. *Journal of Structural Geology*, *30*(1), 50–64. https://doi.org/10.1016/j.jsg.2007.10.005

Questiaux, J. M., Couples, G. D., & Ruby, N. (2010). Fractured reservoirs with fracture corridors. *Geophysical Prospecting*, *58*(2), 279–295. https://doi.org/10.1111/j.1365-2478.2009.00810.x

Ravnås, R., & Bondevik, K. (1997). Architecture and controls on Bathonian–Kimmeridgian shallow-marine synrift wedges of the Oseberg–Brage area, northern North Sea. *Basin Research*, *9*(3), 197–226. https://doi.org/10.1046/j.1365-2117.1997.00041.x

Reeve, M. T., Bell, R. E., Duffy, O. B., Jackson, C. A. L., & Sansom, E. (2015). The growth of non-colinear normal fault systems; what can we learn from 3D seismic reflection data? *Journal of Structural Geology*, *70*, 141–155. https://doi.org/10.1016/j.jsg.2014.11.007

Reeve, M. T., Bell, R. E., & Jackson, C. A.-L. (2013). Origin and significance of intra-basement seismic reflections offshore western Norway. *Journal of the Geological Society*, *171*(1), 1–4. https://doi.org/10.1144/jgs2013-020

Riber, L., Dypvik, H., & Senile, R. (2015). Altered basement rocks on the Utsira high and its surroundings, Norwegian North Sea. *Norwegian Journal of Geology*, *95*(1), 57–89. https://doi.org/10.17850/njg95-1-04

Richards, F. L., Richardson, N. J., Bond, C. E., & Cowgill, M. (2015). Interpretational variability of structural traps: Implications for exploration risk and volume uncertainty. *Geological Society, London, Special Publications*, *421*(1), 7–27. https://doi.org/10.1144/sp421.13

Roberts, A., Yielding, G., Kusznir, N., Walker, I., & Dorn-Lopez, D. (1995). Quantitative analysis of triassic extension in the northern Viking graben. *Journal of the Geological Society*, *152*(1), 15–26. https://doi.org/10.1144/gsjgs.152.1.0015

Robson, D. A. (1971). The structure of the Gulf of Suez (Clysmic) rift, with special reference to the eastern side. *Journal of the Geological Society*, *127*(3), 247–271. https://doi.org/10.1144/gsjgs.127.3.0247

Sanderson, D. J., & Nixon, C. W. (2015). The use of topology in fracture network characterization. *Journal of Structural Geology*, *72*, 55–66. https://doi.org/10.1016/j.jsg.2015.01.005

Sanderson, D. J., & Nixon, C. W. (2018). Topology, connectivity and percolation in fracture networks. *Journal of Structural Geology*, *115*, 167–177. https://doi.org/10.1016/j.jsg.2018.07.011

Sanderson, D. J., Peacock, D. C., Nixon, C. W., & Rotevatn, A. (2019). Graph theory and the analysis of fracture networks. *Journal of Structural Geology*, *125*, 155–165. https://doi.org/10.1016/j.jsg.2018.04.011

Sherman, S., Dem'Yanovich, V., & Lysak, S. (2004). Active faults, seismicity and recent fracturing in the lithosphere of the Baikal rift system. *Tectonophysics*, *380*(3–4), 261–272. https://doi.org/10.1016/j.tecto.2003.09.023

Slagstad, T., Davidsen, B., & Daly, J. S. (2011). Age and composition of crystalline basement rocks on the Norwegian continental margin: Offshore extension and continuity of the Caledonian–Appalachian orogenic belt. *Journal of the Geological Society*, *168*(5), 1167–1185. https://doi.org/10.1144/0016-76492010-136

Ter Voorde, M., Færseth, R., Gabrielsen, R., & Cloetingh, S. (2000). Repeated lithosphere extension in the northern Viking graben: A coupled or a decoupled rheology? *Geological Society, London, Special Publications*, *167*(1), 59–81. https://doi.org/10.1144/gsl.sp.2000.167.01.04

Terzaghi, R. D. (1965). Sources of error in joint surveys. *Géotechnique*, *15*(3), 287–304. https://doi.org/10.1680/geot.1965.15.3.287

Tillmans, F. (2020). *Deep-water syn-rift sedimentation and tectonics: The late Jurassic of the Lomre and uer terraces, northern North Sea.* (PhD Thesis). University of Bergen.

Tillmans, F., Gawthorpe, R. L., Jackson, C. A. L., & Rotevatn, A. (2021). Syn-rift sediment gravity flow deposition on a Late Jurassic fault-terraced slope, northern North Sea. *Basin Research*, *33*(3), 1844–1879. https://doi.org/10.1111/bre.12538

Torsvik, T. H., Andersen, T. B., Eide, E. A., & Walderhaug, H. J. (1997). The age and tectonic significance of dolerite dykes in western Norway. *Journal of the Geological Society*, *154*(6), 961–973. https://doi.org/10.1144/gsjgs.154.6.0961

Underhill, J. R., & Partington, M. (1993). Jurassic thermal doming and deflation in the North Sea: Implications of the sequence stratigraphic evidence. In *Paper presented at the geological society, London, petroleum geology conference series.*

Valle, P., Færseth, R. B., & Fossen, H. (2002). Devonian-Triassic brittle deformation based on dyke geometry and fault kinematics in the Sunnhordland region, SW Norway. *Norwegian Journal of Geology/Norsk Geologisk Forening*, *82*(1), 3–17.

Vermilye, J. M., & Scholz, C. H. (1998). The process zone: A microstructural view of fault growth. *Journal of Geophysical Research*, *103*(B6), 12223–12237. https://doi.org/10.1029/98jb00957

Watterson, J., Walsh, J., Gillespie, P., & Easton, S. (1996). Scaling systematics of fault sizes on a large-scale range fault map. *Journal of Structural Geology*, *18*(2–3), 199–214. https://doi.org/10.1016/s0191-8141(96)80045-9

Wiest, J., Jacobs, J., Fossen, H., Ganerød, M., & Osmundsen, P. (2021). Segmentation of the Caledonian orogenic infrastructure and exhumation of the Western Gneiss Region during transtensional collapse. *Journal of the Geological Society*, *178*(3), jgs2020-199. https://doi.org/10.1144/jgs2020-199

Wiest, J., Wrona, T., Bauck, M. S., Fossen, H., Gawthorpe, R., Osmundsen, P. T., & Faleide, J. I. (2020). From Caledonian collapse to North Sea rift: The extended history of a metamorphic core complex. *Tectonics*, *39*(10), e2020TC006178. https://doi.org/10.1029/2020tc006178

Withjack, M. O., Schlische, R. W., & Olsen, P. E. (2002). Rift-basin structure and its influence on sedimentary systems.

Wrona, T., Pan, I., Bell, R., Jackson, C. A.-L., Gawthorpe, R., Fossen, H., et al. (2022). Complex fault system revealed from 3-D seismic reflection data with deep learning and fault network analysis. *EGUsphere*, *2022*, 1–22. https://doi.org/10.5194/egusphere-2022-1190

Wu, L., Thorsen, R., Ottesen, S., Meneguolo, R., Hartvedt, K., Ringrose, P., & Nazarian, B. (2021). Significance of fault seal in assessing CO2 storage capacity and containment risks–an example from the Horda Platform, northern North Sea. *Petroleum Geoscience*, *27*(3), petgeo2020-2102. https://doi.org/10.1144/petgeo2020-102

Ziegler, P. (1975). Geologic evolution of North Sea and its tectonic framework. *AAPG Bulletin*, *59*(7), 1073–1097.

Ziegler, P. (1990). Tectonic and palaeogeographic development of the North Sea rift system. In *Tectonic evolution of the North Sea rifts* (Vol. 81, pp. 1–36). Oxford Science Publications.

Ziegler, P. (1992). North Sea rift system. In P. A. Ziegler (Ed.), *Geodynamics of rifting, volume I. Case history studies on rifts: Europe and Asia. Tectonophysics* (Vol. 208, pp. 55–75).